AIMS Mathematics, 11(9): 28547–28581.
DOI: 10.3934/math.20261137
Received: 19 June 2026
Revised: 11 August 2026
Accepted: 21 August 2026
Published: 07 September 2026

http://www.aimspress.com/journal/Math

Research article

Dynamics, bifurcations, and machine learning-based analysis of a nonstandard discrete predator-prey model with predator harvesting

Asifa Tassaddiq[1], Rizwan Ahmed[2], Rabab Alharbi[3], Dalal Khalid Almutairi[4], Ruhaila Md Kasmani[5], Youngmoon Lee[6,7,*] and Jawad Khan[8,*]

[1] Department of Information Technology, College of Computer and Information Sciences, Majmaah University, Al Majmaah 11952, Saudi Arabia
[2] International Center for Interdisciplinary Research in Sciences, The University of Lahore, Lahore, Pakistan
[3] Department of Mathematics, College of Science, Qassim University, Buraydah 51452, Saudi Arabia
[4] Department of Mathematics, College of Science, Al-Zulfi, Majmaah University, Al-Majmaah 11952, Saudi Arabia
[5] Institute of Mathematical Sciences, Universiti Malaya, Kuala Lumpur 50603, Malaysia
[6] Department of Robotics, Hanyang University, Ansan 15588, Republic of Korea
[7] Department of Applied AI, Hanyang University, Ansan 15588 Republic of Korea
[8] School of Computing, Gachon University, Seongnam 13120, Republic of Korea

* **Correspondence:** Email: youngmoonlee@hanyang.ac.kr, jkhanbk1@gachon.ac.kr.

Abstract: This paper investigates the dynamics of a predator-prey model with predator harvesting using a Mickens-type nonstandard finite difference (NSFD) scheme. The proposed discrete model preserves positivity and biological feasibility. The existence and local stability of the equilibrium points are analyzed, and conditions for transcritical and Neimark–Sacker bifurcations are derived. The direction and stability of the Neimark–Sacker bifurcation are determined using normal form theory. In contrast to the corresponding piecewise constant argument discretization, the proposed NSFD model excludes period-doubling and strong resonance bifurcations at the coexistence equilibrium. Decision tree, random forest, and support vector machine methods are also employed to classify the positive equilibrium and long-term dynamical behavior. Numerical simulations support the analytical results. The findings demonstrate that the proposed NSFD scheme provides a dynamically consistent framework for studying discrete predator-prey dynamics with harvesting.

Keywords: predator-prey model; harvesting effect; stability; bifurcation; Lyapunov functions; simulation; machine learning
Mathematics Subject Classification: 39A28, 39A30, 92D25

1. Introduction

Predator-prey interactions constitute a fundamental topic in mathematical ecology and have long served as a cornerstone in the development of nonlinear dynamical systems theory. Starting from the classical models proposed by Lotka and Volterra [1, 2], mathematical formulations of interacting species have greatly contributed to the understanding of population oscillations, stability characteristics, and the emergence of complex temporal dynamics. Over time, these classical frameworks have been progressively extended to incorporate a broader spectrum of ecological factors, such as nonlinear functional responses [3, 4], prey refuges [5, 6], harvesting mechanisms [7], Allee effects [8], cannibalism [9], and predator-induced fear effects [10]. As a result of these continual developments, predator-prey models continue to attract substantial attention and remain a vibrant area of research linking applied mathematics, nonlinear dynamics, and ecological theory.

Predator-prey systems in continuous time systems have traditionally been modeled by ordinary differential equations, which have been extensively studied by means of qualitative dynamics, bifurcation theory, and perturbation methods. These investigations have revealed that the dominant growth rates, predation pressures, and mortality rates determine the long-term system dynamics, including coexistence, extinction, and oscillations. The analysis reveals that there are several ecological processes that occur at discrete times. Seasonal growth, periodic harvesting, generational turnover, and discrete population observations demand discrete-time models. Discrete dynamical systems have more possibilities for behavior than continuous systems because they can produce quasiperiodic oscillations, closed invariant orbits, and complex bifurcation structures.

The development of predator-prey models using discrete-time approaches demands more than the basic numerical procedures, as the discretization process has a direct effect on the final dynamical behavior. One of the most common techniques used to develop discrete-time models involves the derivation of discrete models from continuous systems using basic numerical methods such as the forward Euler scheme [11]. While these numerical methods are straightforward to apply, the basic discretization approach often fails to retain the important characteristics of the system as described in the continuous model. This can result in the development of an ecological model that generates results that are not biologically feasible, resulting in oscillations, bifurcations, and negative population densities.

To overcome these limitations, the nonstandard finite difference (NSFD) method, introduced by Mickens [12, 13], provides an effective approach for discretizing nonlinear differential equations. The basic idea behind NSFD schemes is to ensure the preservation of critical qualitative properties of the original continuous systems, independent of the discretization step size. The above aim is accomplished through the application of nonlocal approximations of the nonlinear terms, along with the development of specific denominator functions that determine the discrete derivatives. In population dynamics studies, NSFD discretization schemes provide three primary advantages, which include the preservation of positivity, reduced instabilities, and the correct modeling of equilibrium states with their stability properties. As a result, NSFD-based discrete systems provide a reliable platform for studying long-term ecological dynamics.

Discrete predator-prey models developed by using NSFD methods have garnered considerable

attention due to their ability to maintain the qualitative essence of the original continuous models. For example, Moghadas et al. [14] developed a discretization scheme for a generalized Gause-type predator-prey model using the NSFD method and demonstrated the ability of the scheme to capture the qualitative features of the system, including a supercritical Hopf bifurcation, while the Euler/RK methods fail to do so. Bairagi and Biswas [15] have demonstrated the dynamical consistency of the NSFD method for any step size, unlike the Euler method, which leads to spurious chaotic dynamics. Shabbir et al. [16] developed a dynamically consistent NSFD method and demonstrated the occurrence of a Neimark-Sacker (NS) bifurcation, which is the counterpart of a Hopf bifurcation in the original continuous system. In addition, Dang and Hoang [17] have demonstrated the ability of the NSFD method to maintain the positive and stable nature of the system even for larger step sizes, while the traditional methods fail to perform well. The stability characteristics and NS bifurcation in an NSFD model of the Lotka-Volterra system, with the incorporation of hybrid control strategies, have been studied in the recent paper by Ahmed et al. [18]. In a more recent paper, Kome and Yazlik [19] introduced a discrete model using NSFD with prey immigration, stability, supercritical NS bifurcation, and feedback control to prevent chaotic behavior, as NSFD avoids the flip bifurcation occurring in the discretization using the Euler method.

Recently, machine learning techniques have also begun to provide useful complementary tools for nonlinear dynamical systems [20, 21]. In ecological models, however, their use for predicting stability types, bifurcation-related transitions, and long-term dynamical regimes is still relatively limited. Motivated by this gap, the present work combines analytical bifurcation theory with supervised machine learning methods. In particular, decision tree, random forest, and support vector machine (SVM) classifiers are used to predict the topological type of the coexistence equilibrium and the long-term dynamical response of the system over large parameter domains.

Motivated by the preceding discussion, this study focuses on the discrete-time formulation and dynamical investigation of a predator-prey system obtained from the following continuous-time model [22]:

$$\begin{cases} \dfrac{\mathrm{d}x}{\mathrm{d}t} = \alpha x(1-x) - \gamma xy, \\ \dfrac{\mathrm{d}y}{\mathrm{d}t} = \beta xy - \eta y - hy. \end{cases} \tag{1.1}$$

In system (1.1), the variables $x(t)$ and $y(t)$ represent the densities of the prey and predator populations, respectively. The constant $\alpha > 0$ denotes the intrinsic growth rate of the prey, and the nonlinear term $\alpha x(1-x)$ models logistic growth with the carrying capacity scaled to one. The parameter $\gamma > 0$ characterizes the predation or attack rate, reflecting the strength of predator impact on the prey, with the bilinear term γxy accounting for prey removal through predator-prey interactions. In the predator dynamics, $\beta > 0$ corresponds to the conversion efficiency, or reproductive gain of predators resulting from prey consumption, so that βxy describes predator population increase supported by available prey. The constant $\eta > 0$ characterizes the predator death rate when prey are unavailable, whereas $h > 0$ measures the strength of harvesting pressure acting proportionally on the predator population. Specifically, the harvesting term $-hy$ implies that predators are removed at a rate proportional to their current density $y(t)$.

Specifically, system (1.1) was discretized and examined in [22] through the piecewise constant argument technique. A notable benefit of this discretization is its ability to preserve positivity,

thereby guaranteeing that population variables remain nonnegative. Although the method has its own advantages, it has a major drawback in the sense that it may lead to period-doubling (PD) bifurcation, resonance, and chaotic behavior, although these phenomena cannot be present in the planar autonomous continuous-time system (1.1). Therefore, any type of chaos appearing due to the discretization procedure should be treated as a numerical artifact rather than a genuine ecological phenomenon. The presence of such artificial dynamics may lead to the wrong understanding of extinction, persistence, and coexistence.

Recent investigations have revealed that certain discrete-time predator-prey models, especially those formulated using the piecewise constant argument (PCA) method, exhibit highly complex dynamics, such as PD bifurcation, codimension-two bifurcation, and chaotic behavior. The bifurcation analysis of a discrete prey-predator model was performed by Sharma et al. [23], where fold, flip, and NS bifurcation, as well as codimension-two bifurcation of (1:2, 1:3, 1:4) types, were revealed using normal form analysis. Aldosary and Ahmed [24] used the PCA method to discretize a Leslie-type model, which exhibited PD and NS bifurcations. Chaotic behavior was revealed in predator-prey dynamics by calculating the Lyapunov exponents. The chaotic behavior was effectively eliminated by using feedback and hybrid control schemes. Ishaque et al. [25] extended a discrete predator-prey model with the inclusion of fear factors, derived conditions for PD and NS bifurcations, and implemented chaos control. The authors also included experimental observations to validate the theory. Liu et al. [26] studied the discretization of the PCA model with a Holling type IV response function. They also identified flip, NS, and codimension-two resonance bifurcations, which resulted in quasiperiodic and chaotic attractors. In another study, Ishaque and Din [27] proposed a PCA model based on the Leslie-Gower model with prey refuge. They also identified the destabilizing effect of refuge through PD, NS, and higher codimension bifurcations. They also identified chaos in the model with the help of Lyapunov and Kaplan-Yorke dimensions.

The above findings reveal an important and practically relevant gap in the literature, namely, the need to construct a discrete analogue of system (1.1) with positive solutions and with reduced risk of discretization-induced artificial dynamics, especially PD bifurcations and related spurious oscillatory behavior. In other words, the main challenge here is to design a reliable discrete model that can capture the true dynamics of the underlying continuous ecological system.

In order to address this issue, a Mickens-inspired NSFD discretization of system (1.1) is formulated. Consistent with the design rules of NSFD methods, the standard discretized derivative is replaced with a denominator that depends on the time step $\sigma > 0$, and nonlinear interactions are addressed through suitable nonlocal discretizations. As a result, we obtain the following NSFD scheme:

$$\begin{cases} \dfrac{x_{n+1} - x_n}{\sigma} = \alpha x_n - \alpha x_n x_{n+1} - \gamma x_{n+1} y_n, \\ \dfrac{y_{n+1} - y_n}{\sigma} = \beta x_n y_n - \eta y_{n+1} - h y_{n+1}. \end{cases} \tag{1.2}$$

The scheme can be expressed in the following explicit form:

$$\begin{cases} x_{n+1} = \dfrac{(1 + \alpha\sigma)x_n}{1 + \alpha\sigma x_n + \gamma\sigma y_n}, \\ y_{n+1} = \dfrac{y_n + \beta\sigma x_n y_n}{1 + (h + \eta)\sigma}. \end{cases} \tag{1.3}$$

The proposed NSFD scheme preserves positivity. Indeed, if $x_n > 0$ and $y_n > 0$, then the right-hand sides of (1.3) are strictly positive, implying that $x_{n+1} > 0$ and $y_{n+1} > 0$. Hence, positive initial conditions generate positive solutions for all $n \geq 0$, ensuring the biological feasibility of the model. Moreover, the denominators of the update functions satisfy

$$1 + \alpha\sigma x_n + \gamma\sigma y_n > 1, \qquad 1 + (h + \eta)\sigma > 1,$$

for all admissible parameter values and positive states. Hence, the map is well defined at every iteration and cannot develop singularities. Consequently, finite-time blow-up is excluded within the positive quadrant.

The main contributions and novel aspects of this study can be summarized as follows:

- A Mickens-type NSFD scheme is proposed for the continuous predator-prey model (1.1), and an explicit nonlinear discrete dynamical system (1.3) is obtained.
- The proposed NSFD scheme guarantees that the populations remain nonnegative and physically feasible at each step.
- Unlike the PCA-based discrete model analyzed in [22], the proposed NSFD model does not exhibit discretization-induced PD bifurcation and strong resonance bifurcations.
- The local stability criteria for all fixed points are rigorously proven.
- The existence and direction of stability of a transcritical bifurcation at the boundary equilibrium and an NS bifurcation at the interior coexistence equilibrium are shown, along with the stability being determined via the first Lyapunov coefficient.
- Three machine learning techniques, decision tree, random forest, and SVM, are implemented to classify the positive fixed point.
- Numerical simulations substantiate the theoretical results via bifurcation diagrams, phase plane plots, and Lyapunov exponent computations.

The layout of the paper is arranged as follows. In Section 2, we first determine all equilibria of system (1.3) and then examine their local stability through eigenvalue analysis of the associated Jacobian matrix. Section 3 is devoted to bifurcation phenomena, where transcritical and NS bifurcations are studied using center manifold arguments and normal form computations. Section 4 investigates three machine learning techniques for classification of the positive fixed point. Section 5 presents numerical simulations that illustrate the analytical results and display the typical dynamical behavior of system (1.3). The main findings of the paper are summarized in Section 6.

2. Topological characterization of equilibrium points

Equilibrium stability analysis is the basis for predator-prey system studies using qualitative research methodology. Equilibrium points are the points where the predator and prey populations remain constant. The determination of the stability of an equilibrium point helps scientists predict changes in the populations while offering vital information on the parameters that govern the system.

2.1. Existence of fixed points

The equilibrium solutions (x, y) of model (1.3) are determined by solving the following system:

$$\begin{cases} x = \dfrac{(1+\alpha\sigma)x}{1+\alpha\sigma x+\gamma\sigma y}, \\ y = \dfrac{y+\beta\sigma xy}{1+(h+\eta)\sigma}. \end{cases} \tag{2.1}$$

It follows that the discrete model (1.3) possesses three fixed points given by

$$E_0 = (0,0),\ E_1 = (1,0),\ E^* = \left(\frac{\eta+h}{\beta}, \frac{\alpha(\beta-\eta-h)}{\beta\gamma}\right).$$

The trivial equilibrium point E_0 and the boundary equilibrium point E_1 exist for every feasible set of parameter values. The existence of the unique positive fixed point at the coexistence equilibrium E^* requires that $\beta > \eta + h$. The equilibrium point $E_0 = (0,0)$ represents the extinction of both species, whereas $E_1 = (1,0)$ corresponds to the scenario in which all predators die out while the prey population reaches its maximum sustainable level. Biologically, the condition $\beta > \eta + h$ must be satisfied for predators to persist in the system. In particular, the parameter β measures the per-capita contribution to predator growth arising from prey intake, whereas the term $\eta + h$ captures the combined per-capita reduction caused by natural death and harvesting. Consequently, if $\beta \leq \eta + h$, predator growth is insufficient to offset losses, making coexistence impossible; in contrast, when $\beta > \eta + h$, the existence of a biologically meaningful positive coexistence equilibrium is ensured. Furthermore, because harvesting contributes additively to mortality in the predator dynamics, larger values of h push the system closer to predator extinction and may undermine coexistence by lowering the predators' effective net growth rate.

2.2. Stability of fixed points

To determine the local nature of the equilibrium points, we follow the analytical framework adopted in [28]. By computing the first-order partial derivatives, the Jacobian matrix of the system evaluated at a general fixed point (x, y) is obtained as

$$J(x,y) = \begin{bmatrix} \frac{(1+\alpha\sigma)(1+y\gamma\sigma)}{(1+x\alpha\sigma+y\gamma\sigma)^2} & -\frac{\gamma\sigma(x+x\alpha\sigma)}{(1+x\alpha\sigma+y\gamma\sigma)^2} \\ \frac{y\beta\sigma}{1+(h+\eta)\sigma} & \frac{1+x\beta\sigma}{1+(h+\eta)\sigma} \end{bmatrix}.$$

The eigenvalues of $J(E_0)$ are $\xi_1 = 1 + \alpha\sigma$ and $\xi_2 = \frac{1}{1+(h+\eta)\sigma}$. Clearly, $\xi_1 > 1$ and $\xi_2 < 1$. Thus, E_0 is a saddle point. This classification is consistent with the corresponding result reported in [22].

Proposition 2.1. *E_1 is*

1. *a sink if $\beta < h + \eta$,*
2. *never a source,*
3. *a saddle if $\beta > h + \eta$,*
4. *non-hyperbolic, and model* (1.3) *experiences transcritical bifurcation at E_1 if $\beta = h + \eta$.*

Proof. The Jacobian matrix associated with system (1.3), when evaluated at the boundary equilibrium point E_1, is given by

$$J(E_1) = \begin{bmatrix} \frac{1}{1+\alpha\sigma} & -\frac{\gamma\sigma}{1+\alpha\sigma} \\ 0 & \frac{1+\beta\sigma}{1+(h+\eta)\sigma} \end{bmatrix}.$$

Since $J(E_1)$ is an upper triangular matrix, its eigenvalues are given by the diagonal entries $\xi_1 = \frac{1}{1+\alpha\sigma}$ and $\xi_2 = \frac{1+\beta\sigma}{1+(h+\eta)\sigma}$. It is immediate that $\xi_1 < 1$. Furthermore,

$$|\xi_2| \begin{cases} < 1, & \text{if } \beta < h + \eta, \\ = 1, & \text{if } \beta = h + \eta, \\ > 1, & \text{if } \beta > h + \eta. \end{cases} \tag{2.2}$$

□

Next, we evaluate the Jacobian matrix of the system at the interior equilibrium point E^*, which takes the form

$$J(E^*) = \begin{bmatrix} \frac{\beta+\alpha\beta\sigma-\alpha(h+\eta)\sigma}{\beta+\alpha\beta\sigma} & -\frac{\gamma(h+\eta)\sigma}{\beta+\alpha\beta\sigma} \\ -\frac{\alpha(h-\beta+\eta)\sigma}{\gamma+\gamma(h+\eta)\sigma} & 1 \end{bmatrix}. \tag{2.3}$$

The characteristic equation associated with the Jacobian matrix $J(E^*)$ can be written as

$$\Lambda(\xi) = \xi^2 + K_1\xi + K_0,$$

where

$$K_1 = \frac{-2\beta + \alpha(h - 2\beta + \eta)\sigma}{\beta + \alpha\beta\sigma},$$
$$K_0 = \frac{\beta + \beta(h + \alpha + \eta)\sigma + 2\alpha\beta(h + \eta)\sigma^2 + \alpha(h + \eta)\sigma(-1 - 2(h + \eta)\sigma)}{\beta(1 + \alpha\sigma)(1 + (h + \eta)\sigma)}.$$

It follows from direct computations that

$$\Lambda(0) = \frac{\beta + \beta(h + \alpha + \eta)\sigma + 2\alpha\beta(h + \eta)\sigma^2 + \alpha(h + \eta)\sigma(-1 - 2(h + \eta)\sigma)}{\beta(1 + \alpha\sigma)(1 + (h + \eta)\sigma)},$$
$$\Lambda(-1) = \frac{\alpha(h + \eta)\sigma(-2 - 3(h + \eta)\sigma) + \beta\left(4 + 4(h + \alpha + \eta)\sigma + 5\alpha(h + \eta)\sigma^2\right)}{\beta(1 + \alpha\sigma)(1 + (h + \eta)\sigma)},$$
$$\Lambda(1) = \frac{\alpha(h + \eta)(\beta - \eta - h)\sigma^2}{\beta(1 + \alpha\sigma)(1 + (h + \eta)\sigma)}.$$

A straightforward evaluation shows that $\Lambda(1) > 0$ and $\Lambda(-1) > 0$. Since $\Lambda(-1) \neq 0$, the value $\xi = -1$ cannot be an eigenvalue of the Jacobian matrix. Consequently, a PD bifurcation does not arise at the coexistence equilibrium E^* of system (1.3). This leads to the following conclusion.

Theorem 2.2. *The positive fixed point E^* is*

1. *a sink if $\beta < 2(h + \eta) + \frac{1}{\sigma}$,*

2. *a source if* $\beta > 2(h+\eta) + \frac{1}{\sigma}$,
3. *never a saddle,*
4. *non-hyperbolic, and model* (1.3) *experiences NS bifurcation at* E^* *if*

$$-2 < \frac{-2\beta + \alpha(h - 2\beta + \eta)\sigma}{\beta + \alpha\beta\sigma} < 2 \text{ and } \beta = 2(h+\eta) + \frac{1}{\sigma}.$$

Remark 2.3. *From a biological perspective, the fact that the eigenvalue* $\xi = -1$ *does not occur at the equilibrium point* E^* *eliminates the standard PD mechanism through which many discrete predator-prey systems exhibit alternating large-small population oscillations and a route to chaotic dynamics. As a result, within the considered NSFD framework, instability of the coexistence equilibrium is expected to be linked to oscillatory behavior through an NS scenario, rather than to sign-changing two-period cycles that often occur as artifacts of numerical discretization.*

Remark 2.4. *From a management perspective, the threshold* $\beta = 2(h+\eta) + \frac{1}{\sigma}$ *can be viewed as a guideline for regulating predator populations in wildlife and fishery systems. Harvesting policies should be designed by considering not only population size, but also the proximity of the system to the bifurcation boundary. Operating close to the threshold may induce long-term oscillations, which can increase the vulnerability of populations to environmental fluctuations, disease outbreaks, or unexpected external disturbances. The derived condition provides a quantitative criterion for identifying parameter regimes that promote stable coexistence and for avoiding management strategies that may trigger undesirable population cycles.*

3. Bifurcation analysis

In this section, we undertake a comprehensive investigation of the bifurcation behavior of system (1.3), focusing particularly on transcritical and NS bifurcations. A comprehensive discussion of the theory underlying bifurcation analysis can be found in [29–31]. Bifurcations serve as critical elements that determine the evolution of the model, as they identify parameter ranges where even small changes can lead to significant transformations in predator-prey interactions. Analysis of bifurcation mechanisms and their respective thresholds offers important insights into ecosystem dynamics, making it easier to design strategies to ensure the long-term survival of predator and prey populations while maintaining ecosystem stability.

3.1. Transcritical bifurcation at E_1

We investigate the transcritical bifurcation occurring at E_1 under condition (4) of Theorem 2.1. The transcritical bifurcation analysis is carried out through a sequence of standard steps. First, the bifurcation parameter is perturbed in a neighborhood of its critical value, and the boundary equilibrium E_1 is translated to the origin. Next, a linear transformation is employed to bring the linear part of the system into a diagonal form and separate the critical eigendirection associated with the unit eigenvalue. The center manifold theorem is then applied to reduce the two-dimensional dynamics to a one-dimensional map on the center manifold. Finally, the reduced map is analyzed using normal form theory to verify the transcritical bifurcation conditions.

Adding a small variation δ into β around $\beta_1 = h + \eta$, the discrete system (1.3) is modified as

$$\begin{cases} x_{n+1} = \dfrac{(1+\alpha\sigma)x_n}{1+\alpha\sigma x_n + \gamma\sigma y_n}, \\ y_{n+1} = \dfrac{y_n + (\beta_1+\delta)\sigma x_n y_n}{1+(h+\eta)\sigma}. \end{cases} \tag{3.1}$$

To facilitate the bifurcation analysis, we shift the boundary equilibrium E_1 to $(0,0)$ by introducing the mapping $\lambda_n = x_n - 1$ and $\mu_n = y_n$. Under this mapping, (3.1) reduces to

$$\begin{bmatrix} \lambda_{n+1} \\ \mu_{n+1} \end{bmatrix} = \begin{bmatrix} \frac{1}{1+\alpha\sigma} & -\frac{\gamma\sigma}{1+\alpha\sigma} \\ 0 & 1 \end{bmatrix} \begin{bmatrix} \lambda_n \\ \mu_n \end{bmatrix} + \begin{bmatrix} \mathbb{F}_1(\lambda_n, \mu_n, \delta) \\ \mathbb{F}_2(\lambda_n, \mu_n, \delta) \end{bmatrix}, \tag{3.2}$$

where

$$\begin{aligned} \mathbb{F}_1(\lambda_n, \mu_n, \delta) &= a_1\lambda_n^2 + a_2\mu_n^2 + a_3\lambda_n\mu_n + a_4\lambda_n^3 + a_5\mu_n^3 + a_6\lambda_n^2\mu_n + a_7\lambda_n\mu_n^2 + O(4), \\ \mathbb{F}_2(\lambda_n, \mu_n, \delta) &= b_1\lambda_n\mu_n + b_2\mu_n\delta + b_3\lambda_n\mu_n\delta + O(4), \end{aligned}$$

$$a_1 = -\frac{\alpha\sigma}{(1+\alpha\sigma)^2},\ a_2 = \frac{\gamma^2\sigma^2}{(1+\alpha\sigma)^2},\ a_3 = \frac{\gamma\sigma(-1+\alpha\sigma)}{(1+\alpha\sigma)^2},\ a_4 = \frac{\alpha^2\sigma^2}{(1+\alpha\sigma)^3},\ a_5 = -\frac{\gamma^3\sigma^3}{(1+\alpha\sigma)^3},$$

$$a_6 = \frac{\alpha\gamma\sigma^2(2-\alpha\sigma)}{(1+\alpha\sigma)^3},\ a_7 = \frac{\gamma^2\sigma^2(1-2\alpha\sigma)}{(1+\alpha\sigma)^3},\ b_1 = \frac{(h+\eta)\sigma}{1+(h+\eta)\sigma},\ b_2 = \frac{\sigma}{1+(h+\eta)\sigma},\ b_3 = \frac{\sigma}{1+(h+\eta)\sigma}.$$

Next, we rewrite system (3.2) in diagonal form using the linear transformation below:

$$\begin{bmatrix} \lambda_n \\ \mu_n \end{bmatrix} = \begin{bmatrix} -\frac{\gamma}{\alpha} & 1 \\ 1 & 0 \end{bmatrix} \begin{bmatrix} \rho_n \\ \kappa_n \end{bmatrix}. \tag{3.3}$$

Applying (3.3) to system (3.2) yields

$$\begin{bmatrix} \rho_{n+1} \\ \kappa_{n+1} \end{bmatrix} = \begin{bmatrix} 1 & 0 \\ 0 & \frac{1}{1+\alpha\sigma} \end{bmatrix} \begin{bmatrix} \rho_n \\ \kappa_n \end{bmatrix} + \begin{bmatrix} \mathbb{G}_1(\rho_n, \kappa_n, \delta) \\ \mathbb{G}_2(\rho_n, \kappa_n, \delta) \end{bmatrix}, \tag{3.4}$$

where

$$\begin{aligned} \mathbb{G}_1(\rho_n, \kappa_n, \delta) &= c_1\rho_n^2 + c_2\rho_n\kappa_n + c_3\rho_n\delta + c_4\rho_n^2\delta + c_5\rho_n\kappa_n\delta + O(4), \\ \mathbb{G}_2(\rho_n, \kappa_n, \delta) &= d_1\rho_n^2 + d_2\kappa_n^2 + d_3\rho_n\kappa_n + d_4\rho_n\delta + d_5\kappa_n^3 + d_6\rho_n^2\delta + d_7\rho_n\kappa_n^2 + d_8\rho_n\kappa_n\delta + O(4), \end{aligned}$$

$$c_1 = -\frac{\gamma(h+\eta)\sigma}{\alpha+\alpha(h+\eta)\sigma},\ c_2 = \frac{(h+\eta)\sigma}{1+(h+\eta)\sigma},\ c_3 = \frac{\sigma}{1+(h+\eta)\sigma},\ c_4 = -\frac{\gamma\sigma}{\alpha+\alpha(h+\eta)\sigma},\ c_5 = \frac{\sigma}{1+(h+\eta)\sigma},$$

$$d_1 = -\frac{\gamma^2(h+\eta)\sigma}{\alpha^2(1+(h+\eta)\sigma)},\ d_2 = -\frac{\alpha\sigma}{(1+\alpha\sigma)^2},\ d_3 = \frac{\gamma\sigma(h+\alpha+\eta+2\alpha(h+\eta)\sigma)}{\alpha(1+\alpha\sigma)(1+(h+\eta)\sigma)},\ d_4 = \frac{\gamma\sigma}{\alpha+\alpha(h+\eta)\sigma},$$

$$d_5 = \frac{\alpha^2\sigma^2}{(1+\alpha\sigma)^3},\ d_6 = -\frac{\gamma^2\sigma}{\alpha^2(1+(h+\eta)\sigma)},\ d_7 = -\frac{\alpha\gamma\sigma^2}{(1+\alpha\sigma)^2},\ d_8 = \frac{\gamma\sigma}{\alpha+\alpha(h+\eta)\sigma}.$$

Next, let Q^C denote the center manifold of (3.4) associated with the origin, considered in a small neighborhood around $\delta = 0$. This manifold can be locally computed by

$$Q^C = \left\{(\rho_n, \kappa_n, \delta) \in \mathbb{R}^3_+ \middle| \kappa_n = p_1\rho_n^2 + p_2\rho_n\delta + p_3\delta^2 + O(3)\right\}.$$

Substituting the center manifold expansion into (3.4), we compare coefficients of like powers of ρ_n and δ to determine the unknown coefficients p_1, p_2, and p_3. We obtain

$$p_1 = -\frac{\gamma^2(h+\eta)(1+\alpha\sigma)}{\alpha^3(1+(h+\eta)\sigma)},\ p_2 = \frac{\gamma+\alpha\gamma\sigma}{\alpha^2(1+(h+\eta)\sigma)},\ p_3 = 0.$$

The center manifold reduction yields the following one-dimensional map:

$$\begin{aligned}\Phi(\rho_n, \delta) := \rho_{n+1} = \rho_n &- \left(\frac{\gamma(h+\eta)\sigma}{\alpha+\alpha(h+\eta)\sigma}\right)\rho_n^2 + \left(\frac{\sigma}{1+(h+\eta)\sigma}\right)\rho_n\delta - \left(\frac{\gamma^2(h+\eta)^2\sigma(1+\alpha\sigma)}{\alpha^3(1+(h+\eta)\sigma)^2}\right)\rho_n^3 \\ &+ \left(\frac{\gamma(h-\alpha+\eta)\sigma}{(\alpha+\alpha(h+\eta)\sigma)^2}\right)\rho_n^2\delta + O(4). \end{aligned} \tag{3.5}$$

Moreover, the reduced map satisfies

$$\Phi(0,0) = 0,\ \Phi_{\rho_n}(0,0) = 1,\ \Phi_{\delta}(0,0) = 0,$$

while the nondegeneracy conditions

$$\Phi_{\rho_n\rho_n}(0,0) = -\frac{2\gamma(h+\eta)\sigma}{\alpha+\alpha(h+\eta)\sigma} \neq 0,\ \Phi_{\rho_n\delta}(0,0) = \frac{\sigma}{1+(h+\eta)\sigma} \neq 0,$$

also hold. As a result, we derive the next conclusion.

Theorem 3.1. *If requirement* (4) *in Theorem 2.1 is satisfied, then* (1.3) *goes through transcritical bifurcation at E_1 if β varies within a small neighborhood of $\beta_1 = h + \eta$.*

Remark 3.2. *The transcritical bifurcation occurring at $\beta = h + \eta$ reflects a stability switch between the predator-free steady state and the coexistence steady state. From a biological standpoint, if the predator conversion efficiency is insufficient, the predator population fails to survive and the dynamics converge to* $(1, 0)$. *However, when β becomes larger than $h + \eta$, a stable coexistence equilibrium appears, implying that predators are able to successfully invade the prey-only setting and ultimately maintain sustained coexistence with the prey population over time.*

3.2. NS bifurcation at E^*

We examine the NS bifurcation at E^* when condition (4) of Theorem 2.2 is satisfied. The NS bifurcation analysis follows a similar procedure. We first perturb the bifurcation parameter near its critical value and translate the equilibrium to the origin. Then, the linear part is transformed into canonical rotational form associated with the complex conjugate eigenvalues. Finally, normal form

theory is applied to compute the first Lyapunov coefficient, which determines the direction and stability of the bifurcating invariant closed curve.

Adding a small variation δ in the bifurcation parameter β near its critical value $\beta_2 = 2(h+\eta) + \frac{1}{\sigma}$ in system (1.3), we obtain

$$\begin{cases} x_{n+1} = \dfrac{(1+\alpha\sigma)x_n}{1+\alpha\sigma x_n + \gamma\sigma y_n}, \\ y_{n+1} = \dfrac{y_n + (\beta_2+\delta)\sigma x_n y_n}{1+(h+\eta)\sigma}. \end{cases} \tag{3.6}$$

We use the mapping $\lambda_n = x_n - \frac{\eta+h}{\beta_2+\delta}$, $\mu_n = y_n - \frac{\alpha(\beta_2+\delta-\eta-h)}{\beta\gamma}$ to translate E^* to the origin. As a result, (3.6) is changed to

$$\begin{bmatrix} \lambda_{n+1} \\ \mu_{n+1} \end{bmatrix} = \begin{bmatrix} \frac{1+\sigma(2h+\alpha+\delta+2\eta+\alpha(h+\delta+\eta)\sigma)}{(1+\alpha\sigma)(1+(2h+\delta+2\eta)\sigma)} & -\frac{\gamma(h+\eta)\sigma^2}{(1+\alpha\sigma)(1+(2h+\delta+2\eta)\sigma)} \\ \frac{\alpha+\alpha(h+\delta+\eta)\sigma}{\gamma+\gamma(h+\eta)\sigma} & 1 \end{bmatrix} \begin{bmatrix} \lambda_n \\ \mu_n \end{bmatrix} + \begin{bmatrix} F(\lambda_n,\mu_n) \\ G(\lambda_n,\mu_n) \end{bmatrix}, \tag{3.7}$$

where

$$\begin{aligned} F(\lambda_n,\mu_n) &= a_1\lambda_n^2 + a_2\mu_n^2 + a_3\lambda_n\mu_n + a_4\lambda_n^3 + a_5\mu_n^3 + a_6\lambda_n^2\mu_n + a_7\lambda_n\mu_n^2 + O(4), \\ G(\lambda_n,\mu_n) &= \Big(\frac{(\delta+2(h+\eta)+\frac{1}{\sigma})\sigma}{1+(h+\eta)\sigma}\Big)\lambda_n\mu_n + O(4). \end{aligned}$$

The detailed forms of the coefficients a_i are given in Appendix A. The local stability and bifurcation behavior of system (3.7) are determined by the eigenvalues of the linearized system. Therefore, we compute the characteristic polynomial of the Jacobian matrix evaluated at the origin, which is given by

$$\xi^2 - p(\delta)\xi + q(\delta) = 0, \tag{3.8}$$

where

$$p(\delta) = \frac{2+2(2h+\alpha+\delta+2\eta)\sigma + \alpha(3h+2\delta+3\eta)\sigma^2}{(1+\alpha\sigma)(1+(2h+\delta+2\eta)\sigma)},$$

$$q(\delta) = \frac{1+\sigma(3h+\alpha+\delta+3\eta+(2h^2+\eta(\delta+2\eta)+\alpha(\delta+3\eta)+h(3\alpha+\delta+4\eta))\sigma+2\alpha(h+\eta)(h+\delta+\eta)\sigma^2)}{(1+\alpha\sigma)(1+(h+\eta)\sigma)(1+(2h+\delta+2\eta)\sigma)}.$$

The roots of Equation (3.8) are given by

$$\xi_{1,2} = \frac{p(\delta)}{2} \pm \frac{i}{2}\sqrt{4q(\delta) - p^2(\delta)}. \tag{3.9}$$

This leads to $|\xi_{1,2}| = \sqrt{q(\delta)}$. Furthermore,

$$\left(\frac{d|\xi_1|}{d\delta}\right)_{\delta=0} = \left(\frac{d|\xi_2|}{d\delta}\right)_{\delta=0} = \frac{\alpha(h+\eta)\sigma^3}{2(1+\alpha\sigma)(1+(h+\eta)\sigma)(1+2(h+\eta)\sigma)} > 0.$$

The positivity of this derivative verifies the transversality condition, ensuring that the eigenvalues cross the unit circle with nonzero speed. In order to exclude strong resonance cases and guarantee the

applicability of the NS bifurcation theorem, the nonresonance condition $\xi_{1,2}^i \neq 1$ for $i = 1, 2, 3, 4$ must also hold at $\delta = 0$. This condition is equivalent to requiring that $p(0) \neq -2, -1, 0, 2$. We verify that under condition (4) of Theorem 2.2,

$$p(0) = \frac{2 + 2(2h + \alpha + 2\eta)\sigma + 3\alpha(h + \eta)\sigma^2}{(1 + \alpha\sigma)(1 + 2(h + \eta)\sigma)} \neq -2, -1, 0, 2.$$

To simplify the bifurcation analysis, we next transform the linear part of system (3.7) into its canonical rotational form corresponding to the complex conjugate eigenvalues on the unit circle. To derive the canonical form of system (3.7) at $\delta = 0$, we apply the following change of variables:

$$\begin{bmatrix} \lambda_n \\ \mu_n \end{bmatrix} = \begin{bmatrix} -\frac{\gamma(h+\eta)\sigma^2}{(1+\alpha\sigma)(1+2(h+\eta)\sigma)} & 0 \\ \frac{\alpha(h+\eta)\sigma^2}{2(1+\alpha\sigma)(1+2(h+\eta)\sigma)} & -\frac{\sigma\sqrt{\alpha(h+\eta)(4+4(2h+\alpha+2\eta)\sigma+7\alpha(h+\eta)\sigma^2)}}{2(1+\alpha\sigma)(1+2(h+\eta)\sigma)} \end{bmatrix} \begin{bmatrix} e_n \\ f_n \end{bmatrix}. \tag{3.10}$$

Under the transformation (3.10), system (3.7) becomes

$$\begin{bmatrix} e_{n+1} \\ f_{n+1} \end{bmatrix} = \begin{bmatrix} \frac{2+2(2h+\alpha+2\eta)\sigma+3\alpha(h+\eta)\sigma^2}{2(1+\alpha\sigma)(1+2(h+\eta)\sigma)} & -\frac{\sigma\sqrt{\alpha(h+\eta)(4+4(2h+\alpha+2\eta)\sigma+7\alpha(h+\eta)\sigma^2)}}{2(1+\alpha\sigma)(1+2(h+\eta)\sigma)} \\ \frac{\sigma\sqrt{\alpha(h+\eta)(4+4(2h+\alpha+2\eta)\sigma+7\alpha(h+\eta)\sigma^2)}}{2(1+\alpha\sigma)(1+2(h+\eta)\sigma)} & \frac{2+2(2h+\alpha+2\eta)\sigma+3\alpha(h+\eta)\sigma^2}{2(1+\alpha\sigma)(1+2(h+\eta)\sigma)} \end{bmatrix} \begin{bmatrix} e_n \\ f_n \end{bmatrix} + \begin{bmatrix} \chi(e_n, f_n) \\ \Upsilon(e_n, f_n) \end{bmatrix}, \tag{3.11}$$

where

$$\chi(e_n, f_n) = c_1 e_n^2 + c_2 f_n^2 + c_3 e_n f_n + c_4 e_n^3 + c_5 f_n^3 + c_6 e_n^2 f_n + c_7 e_n f_n^2 + O(4),$$

$$\Upsilon(e_n, f_n) = d_1 e_n^2 + d_2 f_n^2 + d_3 e_n f_n + d_4 e_n^3 + d_5 f_n^3 + d_6 e_n^2 f_n + d_7 e_n f_n^2 + O(4).$$

The coefficients c_i and d_j are listed in Appendix B. According to the normal form theory for NS bifurcation [30], the direction and stability of the bifurcating invariant closed curve are determined by the first Lyapunov coefficient, which is obtained as

$$L = \left(\left[-Re\left(\frac{(1 - 2\xi_1)\xi_2^2}{1 - \xi_1} \tau_{20}\tau_{11} \right) - \frac{1}{2}|\tau_{11}|^2 - |\tau_{02}|^2 + Re(\xi_2\tau_{21}) \right] \right)_{\delta=0}, \tag{3.12}$$

where

$$\begin{aligned}
\tau_{20} &= \frac{1}{8}\left[\chi_{e_n e_n} - \chi_{f_n f_n} + 2\Upsilon_{e_n f_n} + i(\Upsilon_{e_n e_n} - \Upsilon_{f_n f_n} - 2\chi_{e_n f_n}) \right], \\
\tau_{11} &= \frac{1}{4}\left[\chi_{e_n e_n} + \chi_{f_n f_n} + i(\Upsilon_{e_n e_n} + \Upsilon_{f_n f_n}) \right], \\
\tau_{02} &= \frac{1}{8}\left[\chi_{e_n e_n} - \chi_{f_n f_n} - 2\Upsilon_{e_n f_n} + i(\Upsilon_{e_n e_n} - \Upsilon_{f_n f_n} + 2\chi_{e_n f_n}) \right], \\
\tau_{21} &= \frac{1}{16}\left[\chi_{e_n e_n e_n} + \chi_{e_n f_n f_n} + \Upsilon_{e_n e_n f_n} + \Upsilon_{f_n f_n f_n} + i(\Upsilon_{e_n e_n e_n} + \Upsilon_{e_n f_n f_n} - \chi_{e_n e_n f_n} - \chi_{f_n f_n f_n}) \right].
\end{aligned}$$

The sign of L determines whether the bifurcation is supercritical or subcritical, as well as the stability of the emerging invariant closed curve. On the basis of the preceding analysis, we obtain the following result.

Theorem 3.3. *Suppose condition* (4) *of Theorem 2.2 holds. Provided that the Lyapunov coefficient L in* (3.12) *is nonzero, system* (1.3) *exhibits an NS bifurcation at the interior equilibrium E^* when β varies slightly around $\beta_2 = 2(h+\eta) + \frac{1}{\sigma}$. In addition, $L < 0$ (respectively, $L > 0$) corresponds to a supercritical (respectively, subcritical) bifurcation, producing a single closed invariant curve from E^* that is attracting (respectively, repelling).*

Remark 3.4. *An NS bifurcation identifies the emergence of sustained bounded oscillations in the densities of both species. Ecologically, this transition occurs when the stable coexistence equilibrium becomes unstable and the trajectories approach a closed invariant curve. Such a curve represents recurring predator-prey cycles, which arise due to the discrete-time updating mechanism and the associated delayed density-dependent feedback.*

4. Machine learning-based classification of the positive fixed point

In this section, machine learning techniques are used to classify the behavior of the positive fixed point E^* of system (1.3). Two types of classification problems are considered. First, the local topological nature of E^* is predicted in terms of sink (SK), source (SR), saddle (SD), and nonhyperbolic (NH) behavior. Second, the long-term dynamical response of the system is classified into periodic, quasiperiodic, and chaotic regimes. For both investigations, the model parameters $(\alpha, \beta, \gamma, \eta, \sigma, h)$ are used as input features, while the corresponding dynamical classes are used as output labels.

The purpose of applying machine learning is not to replace the analytical stability and bifurcation results, but to provide a fast computational framework for predicting the behavior of the system over large parameter domains. This is especially useful because direct eigenvalue computations, long-term iterations, and Lyapunov exponent calculations become computationally expensive when a high-dimensional parameter space is explored.

4.1. Topological classification of the positive fixed point

The local behavior of the positive equilibrium E^* is determined by the eigenvalues of the Jacobian matrix evaluated at E^*. Depending on the position of these eigenvalues with respect to the unit circle, the fixed point is classified as sink, source, saddle, or nonhyperbolic. To construct the machine learning dataset, $N = 80000$ random parameter combinations are generated from the interval

$$\alpha, \beta, \gamma, \eta, \sigma, h \in [0.01, 10.5].$$

For each parameter set, the positive equilibrium is computed and the Jacobian matrix is evaluated. The eigenvalues are then used to assign the corresponding topological class. Parameter sets that do not produce a biologically meaningful positive equilibrium are excluded. After filtering, 13, 299 valid samples are retained, consisting of 6 nonhyperbolic point, no saddle points, 10, 298 sinks, and 2995 sources. The dataset is randomly divided into training and testing parts using a $75\% - 25\%$ split.

Three supervised learning methods are applied: decision tree, random forest, and SVM. The decision tree classifier achieves an accuracy of 95.79%. Its confusion matrix and parameter-importance plot are shown in Figure 1. The confusion matrix indicates that most source equilibria are correctly identified, while some misclassifications occur near the boundaries separating different stability classes. The parameter-importance plot shows that h, β, and η have the largest influence on the

classification, with normalized importance values 0.3682, 0.2912, and 0.2838, respectively. In contrast, α and γ have relatively negligible contributions.

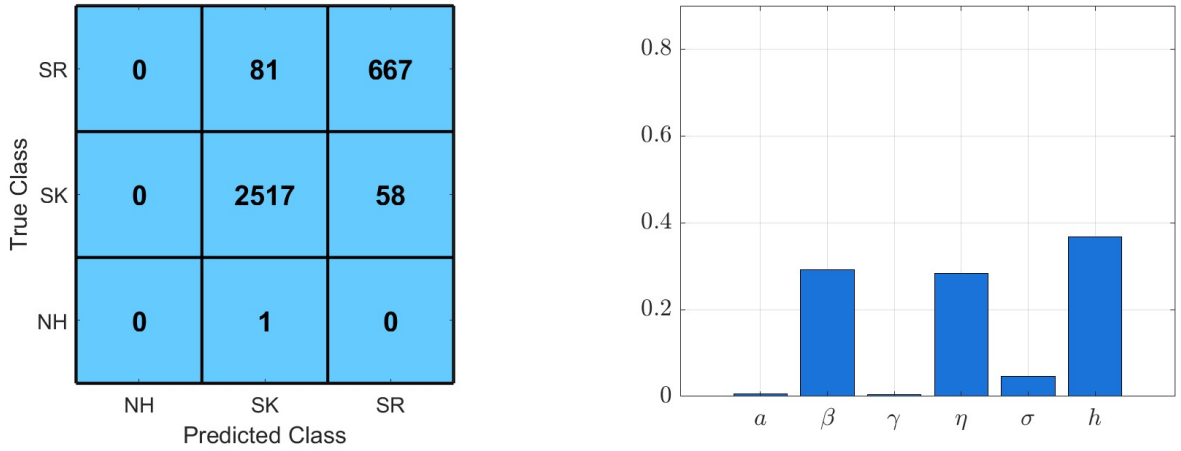

(a) Confusion matrix **(b)** Parameter importance

Figure 1. Decision tree results for topological classification of E^*.

The random forest classifier is constructed using 100 decision trees. It achieves an accuracy of 97.68%, which is higher than that of the single decision tree. The confusion matrix is shown in Figure 2a. The corresponding feature-importance plot in Figure 2b identifies η as the most influential parameter with importance value 0.3916, followed by h with 0.3668 and β with 0.1927. The importance of α (0.0002) and γ (0.0009) is almost negligible, suggesting that it has little effect on the topological classification compared with the other parameters.

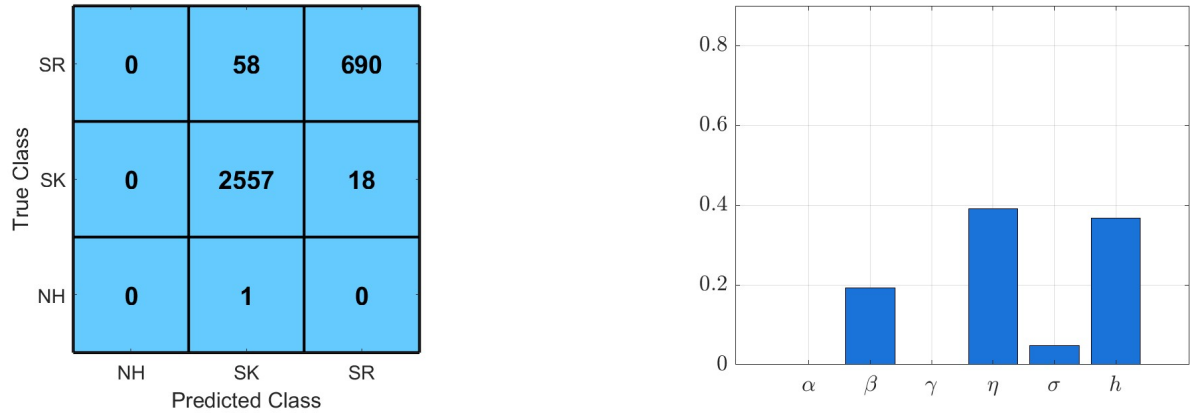

(a) Confusion matrix **(b)** Parameter importance

Figure 2. Random forest results for topological classification of E^*.

The SVM classifier is trained using a radial basis function kernel and a one-versus-all multiclass strategy. It achieves an accuracy of 97.14%. The confusion matrix is given in Figure 3a. Since SVM does not directly provide feature importance, permutation importance is used. The results in Figure 3b

show that η is again the most influential parameter with importance value 0.3955, followed by h with 0.3793 and β with 0.2047. The parameters α and γ have negligible influence.

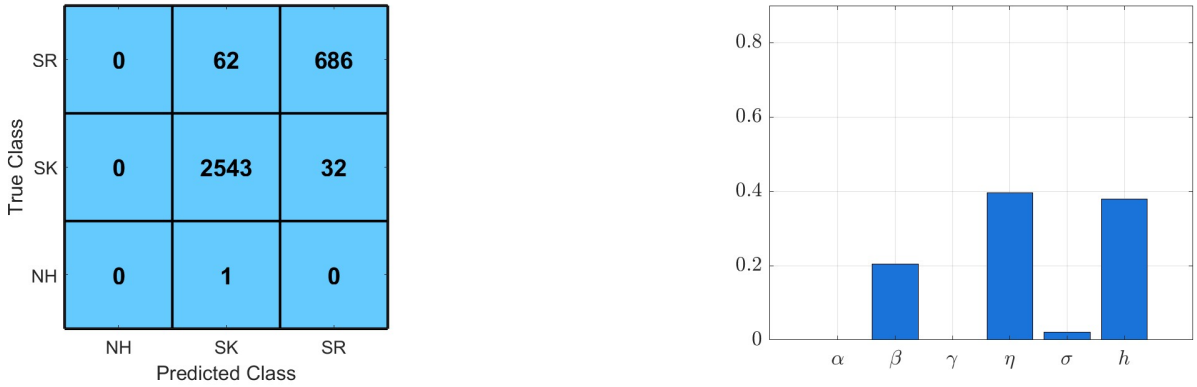

(a) Confusion matrix **(b)** Parameter importance

Figure 3. SVM results for topological classification of E^*.

A comparison of the three methods shows that random forest gives the best performance for topological classification, followed by SVM and decision tree. The accuracy values are summarized as

$$\text{Decision Tree : } 95.79\%, \qquad \text{Random Forest : } 97.68\%, \qquad \text{SVM : } 97.14\%.$$

The feature-importance results are also consistent across the three models. In particular, β, η, and h repeatedly appear among the most influential parameters, whereas α and γ have the weakest contributions. This indicates that β, η, and h play a dominant role in determining whether the positive fixed point behaves as a sink, source, saddle, or nonhyperbolic point.

Remark 4.1. *The dataset used for topological classification is inherently imbalanced due to the analytical properties of system* (1.3)*. In particular, Theorem 2.2 proves that the positive equilibrium E^* can never be a saddle point. Consequently, no saddle samples exist in the admissible parameter space. In addition, nonhyperbolic cases arise exclusively on bifurcation boundaries. Since these boundaries constitute lower-dimensional manifolds within the parameter space, the likelihood of encountering such points through random parameter generation is extremely small. Therefore, the class imbalance observed in the dataset reflects an inherent feature of the underlying dynamical system rather than a limitation of the sampling procedure.*

4.2. Classification of periodic, quasiperiodic, and chaotic dynamics

Next, machine learning is used to classify the long-term dynamical behavior of system (1.3). The objective is to predict whether a given parameter set produces convergence to the positive equilibrium, a periodic orbit, quasiperiodic motion, dynamically different periodic behavior, or chaos.

For this purpose, random parameter values are generated from

$$\alpha, \beta, \gamma, \eta, \sigma, h \in [0.01, 10.50].$$

For each parameter set, system (1.3) is iterated for 15, 000 time steps with initial condition

$$(x_0, y_0) = (0.1, 0.2).$$

The transient part of the trajectory is discarded, and the last 1500 iterates are used for classification. Periodic solutions are detected by comparing the final iterates with previous iterates for the candidate periods

$$p \in \{1, 2, 3, 4, 5, 6, 7, 8, 9, 10, 11, 12, 16, 32, 64\}.$$

If such a repeating pattern is detected, the orbit is assigned to the corresponding periodic class $P - p$. The class $P - 1$ is assigned only when the trajectory converges to the positive equilibrium E^* and the Jacobian eigenvalues confirm its local stability. For trajectories that do not belong to any of the prescribed periodic classes, an extended periodicity test is performed for integer periods up to $p = 375$. If an additional repeating orbit is detected, it is classified as different periodic (DP). Chaotic dynamics are identified when the MLE satisfies MLE $> 10^{-3}$. For trajectories for which no periodicity is detected and $|\text{MLE}| \leq 5 \times 10^{-3}$, an additional power-spectrum analysis is performed to distinguish quasiperiodic motion from unresolved irregular behavior. The power spectra of both state variables are computed using the final trajectory, and the normalized spectral entropy together with the number of significant spectral peaks are evaluated. A trajectory is classified as quasiperiodic (QP) only when no periodicity is detected, the MLE is close to zero, the normalized spectral entropy does not exceed 0.45, and at least two significant spectral peaks are present. A spectral peak is regarded as significant when its power is at least 5% of the maximum spectral power. Parameter combinations corresponding to divergent, numerically invalid, or unresolved trajectories are excluded from the dataset.

The decision tree classifier is first applied to this dynamical classification problem. After filtering invalid and rare cases from 80, 000 total random samples, 12, 548 valid samples are retained. The model achieves an accuracy of 97.19%. The confusion matrix in Figure 4a shows that the dominant classes $P-1$ and QP are classified with high accuracies. Some errors occur among less frequent classes, which is expected due to class imbalance. The parameter-importance plot in Figure 4b indicates parameters β, η, h contribute most strongly to transitions between equilibrium, periodic, quasiperiodic, and dynamically complex regimes.

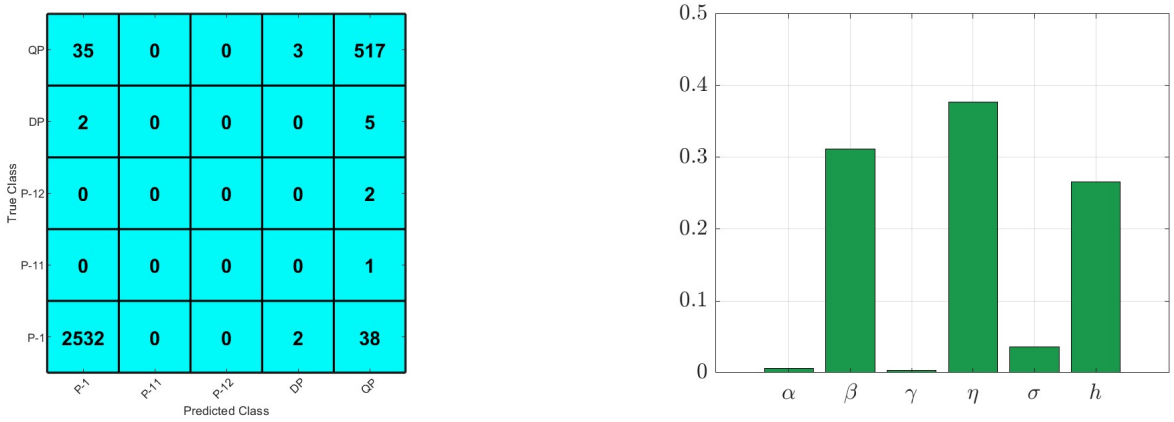

(a) Confusion matrix

(b) Parameter importance

Figure 4. Decision tree results for periodic, quasiperiodic, and chaotic classification.

The random forest model is then trained using 100 trees. From 80,000 randomly generated parameter combinations, 12,554 valid dynamical samples are obtained after filtering. The random forest classifier achieves an accuracy of 98.60%. The confusion matrix is shown in Figure 5a. The feature-importance results in Figure 5b identify the parameters that most strongly affect transitions among stable, periodic, quasiperiodic, and complex motions.

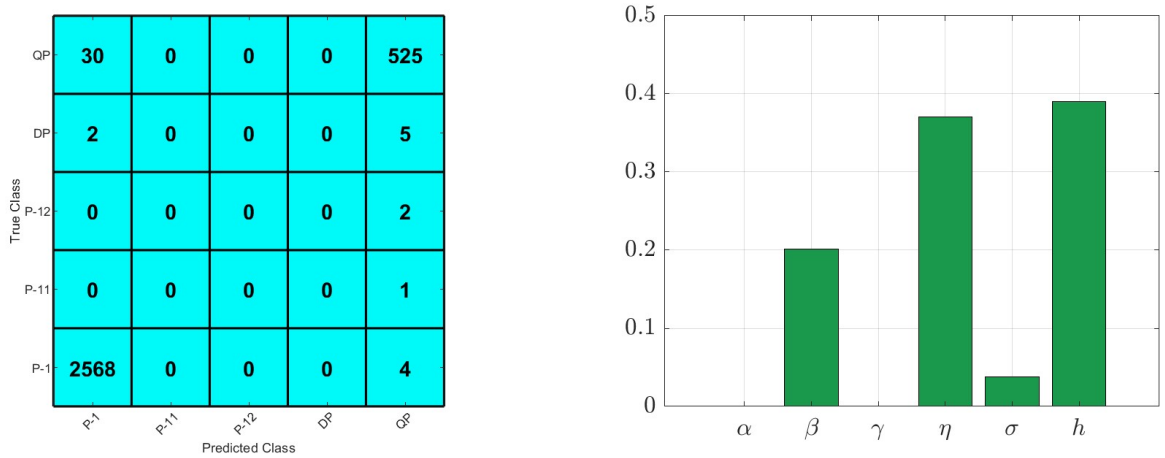

(a) Confusion matrix **(b)** Parameter importance

Figure 5. Random forest results for periodic, quasiperiodic, and chaotic classification.

Finally, the SVM classifier with radial basis function kernel is applied to the same dataset. The model achieves 98.41% accuracy. The confusion matrix in Figure 6a confirms that SVM successfully captures the nonlinear separation between different dynamical classes. The permutation-importance plot in Figure 6b shows the relative effect of each parameter on the classification accuracy.

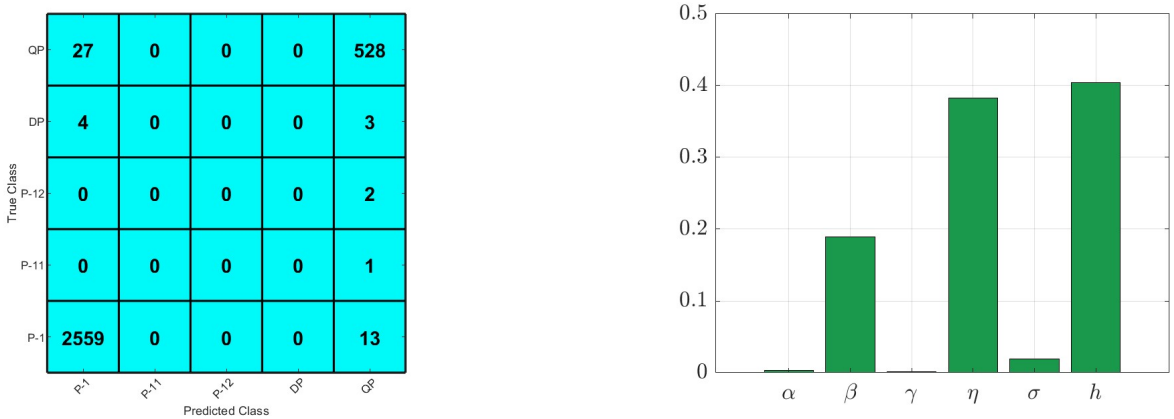

(a) Confusion matrix **(b)** Parameter importance

Figure 6. SVM results for periodic, quasiperiodic, and chaotic classification.

The accuracy comparison for the dynamical classification problem is

Decision Tree : 97.19%, Random Forest : 98.60%, SVM : 98.41%.

All three models provide reliable predictions, while random forest gives the highest accuracy. These results show that machine learning can effectively predict both the local topological type of the positive fixed point and the global dynamical behavior of the system. Therefore, the proposed machine learning framework provides a useful computational tool for exploring large parameter spaces and complements the analytical stability and bifurcation analysis.

5. Numerical simulations

This section presents numerical simulations to demonstrate and support the theoretical findings established in earlier sections. The simulations are designed to confirm the local stability properties of the equilibria, as well as the occurrence of transcritical and NS bifurcations. In order to clarify the complex dynamical behavior of the discrete predator-prey system, we use plots of the bifurcations, phase portraits, time series, and the MLE. The parameter sets used in the numerical simulations are selected hypothetically to satisfy the analytically derived stability and bifurcation conditions and to illustrate the different dynamical regimes of the model.

All numerical simulations are carried out in MATLAB R2023a. In constructing the bifurcation diagrams, the selected bifurcation parameter is varied across the specified interval using 500 uniformly distributed sample points. For each sampled parameter value, system (1.3) is simulated for a total of $N = 8000$ iterations starting from the prescribed initial condition. The initial 7500 iterations are omitted to remove transient dynamics, while the remaining 500 iterates are retained for plotting the bifurcation structure. The phase-plane trajectories are produced with the same initial conditions and simulation horizon, after excluding the first 500 iterations as transient behavior. The MLE is evaluated through the conventional Jacobian-based tangent vector approach, where the perturbation vector is normalized at each iteration to maintain numerical stability. In this computation, the first 800 iterations are disregarded as transients, and the MLE is subsequently approximated using the following 1000 iterations.

5.1. Transcritical bifurcation

Let the parameters be chosen as $\alpha = 0.15, \gamma = 0.35, \eta = 0.75, h = 0.10$, and $\sigma = 0.5$. Under this parameter set, the boundary equilibrium of system (1.3) is given by $E_1 = (1, 0)$. A transcritical bifurcation occurs at E_1 when the bifurcation parameter takes the critical value $\beta_1 = 0.85$. At this point, the eigenvalues of the Jacobean matrix $J(E_1)$ are $\xi_1 = 1$ and $\xi_2 = 0.930233$. Furthermore, detailed computations yield

$$\Phi(e_n, \delta) = e_n - 0.695906e_n^2 + 0.350877e_n\delta - 6.94143e_n^3 + 2.68117e_n^2\delta.$$
$$\Phi(0,0) = 0,\ \Phi_{e_n}(0,0) = 1,\ \Phi_{\delta}(0,0) = 0,$$
$$\Phi_{e_ne_n}(0,0) = -1.39181 \neq 0,\ \Phi_{e_n\delta}(0,0) = 0.350877 \neq 0.$$

This confirms the validity of Theorem 3.1. To provide a visual confirmation of the transcritical bifurcation occurring at E_1, phase portraits are displayed in Figure 7. As shown in Figure 7a, for $\beta = 0.80$, the boundary equilibrium E_1 is locally asymptotically stable, whereas the interior equilibrium E^* is unstable. Figure 7b illustrates that at the critical value $\beta = 0.85$, the equilibria E_1 and E^*

coincide and undergo an exchange of stability. When the parameter is increased to $\beta = 0.90$, Figure 7c reveals that E^* becomes stable and E_1 loses stability. This qualitative change in stability characterizes a transcritical bifurcation.

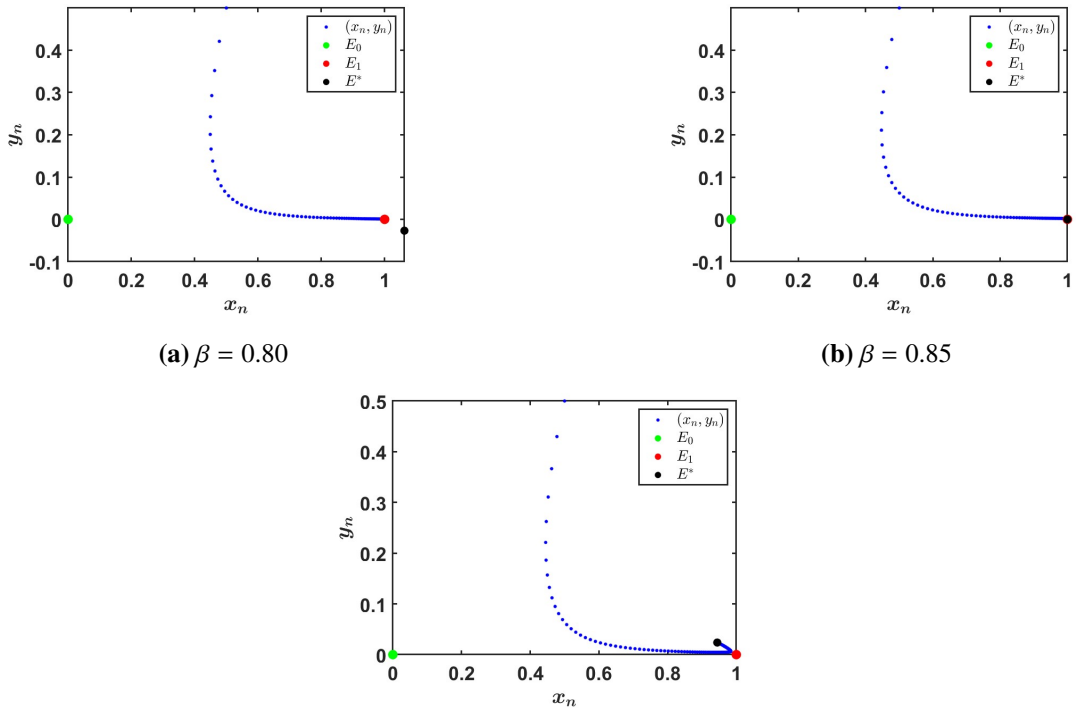

(a) $\beta = 0.80$ **(b)** $\beta = 0.85$

(c) $\beta = 0.90$

Figure 7. Phase portraits of system (1.3) illustrating the transcritical bifurcation with respect to the parameter β.The remaining parameters are fixed at $\alpha = 0.15, \gamma = 0.35, \eta = 0.75, h = 0.10$, and $\sigma = 0.5$, while initial values are chosen as $x_0 = 0.5$ and $y_0 = 0.5$.

Biologically, the parameter β represents the efficiency with which consumed prey is converted into predator growth. Accordingly, the critical threshold $\beta_1 = 0.85$ defines the minimal value required for predator invasion. When $\beta < \beta_1$, the energy acquired through predation is insufficient to compensate for losses due to natural mortality and harvesting, and consequently the predator-free equilibrium $E_1 = (1, 0)$ remains locally stable, inhibiting predator persistence. In contrast, when $\beta > \beta_1$, predators are able to invade the prey-only state successfully, leading to the stabilization of the coexistence equilibrium E^*.

5.2. NS bifurcation analysis varying β

We choose the parameter values $\alpha = 0.95, \gamma = 0.85, \eta = 0.5, h = 0.10$, and $\sigma = 0.65$. In this case, the critical value of the NS bifurcation is $\beta_2 = 2.73846$. The coexistence equilibrium is $E^* = (0.219101, 0.872769)$. Here, the Jacobian matrix has a pair of complex conjugate eigenvalues $\xi_{1,2} = 0.958178 \pm 0.286174i$, which has a modulus of one. In addition, detailed computations yield

$$\tau_{20} = -0.010272 - 0.01737i, \tau_{11} = -0.007143 + 0.005959i,$$
$$\tau_{02} = 0.031102 + 0.027417i, \tau_{21} = 0.001016 + 0.000862i.$$

Consequently, it follows that $L = -0.000664 < 0$, which confirms the assertion of Theorem 3.3. Therefore, the NS bifurcation is of supercritical type, and a closed invariant curve bifurcates from the equilibrium point E^*. The bifurcation diagrams for the values of the parameter β in the interval $[2.15, 3.65]$ are shown in Figure 8a and 8b. In addition, the corresponding MLE plot is shown in Figure 8c. In general, the negative values of the MLE function indicate the trajectories that converge to a stable fixed point or a stable periodic orbit. On the other hand, the positive values of the MLE function indicate sensitive dependence on the initial conditions, which is a characteristic of chaotic behavior. In the current study, the calculated values of the MLE function are zero or very close to zero, which indicates that the system does not have chaotic behavior for this parameter range.

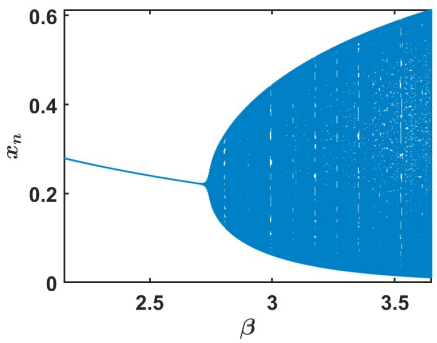

(a) Bifurcation diagram of x_n

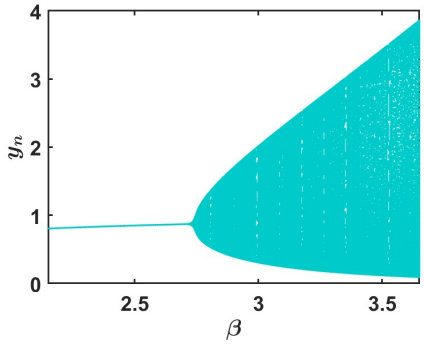

(b) Bifurcation diagram of y_n

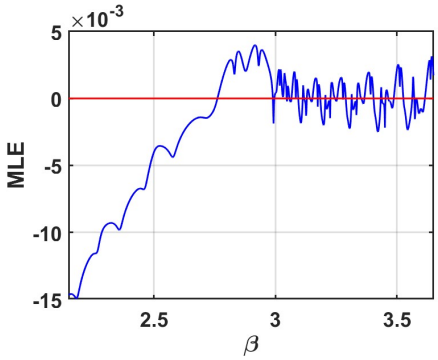

(c) MLE plot

Figure 8. Bifurcation diagrams together with the corresponding MLE plot of system (1.3) as the parameter β varies. The parameters are fixed at $\alpha = 0.95, \gamma = 0.85, \eta = 0.5, h = 0.10$, and $\sigma = 0.65$, with initial conditions selected as $x_0 = 0.2, y_0 = 0.9$.

Next, Figure 9a–9i present the phase portraits of system (1.3) for different values of β. These phase portraits indicate that the coexistence equilibrium point E^* is a sink if $\beta < 2.73846$, but undergoes NS bifurcation at $\beta = 2.73846$, beyond which it loses stability. Moreover, from the three-dimensional phase portrait in Figure 9j, it is obvious that the radius of the invariant curve increases with the increase of the parameter β. Therefore, from the management point of view, it can be concluded that higher predator efficiency, in other words, higher β, can destabilize the coexistence equilibrium point. From the ecological point of view, the oscillations in the population dynamics can be considered as boom-bust cycles, which can increase the risk of extinction.

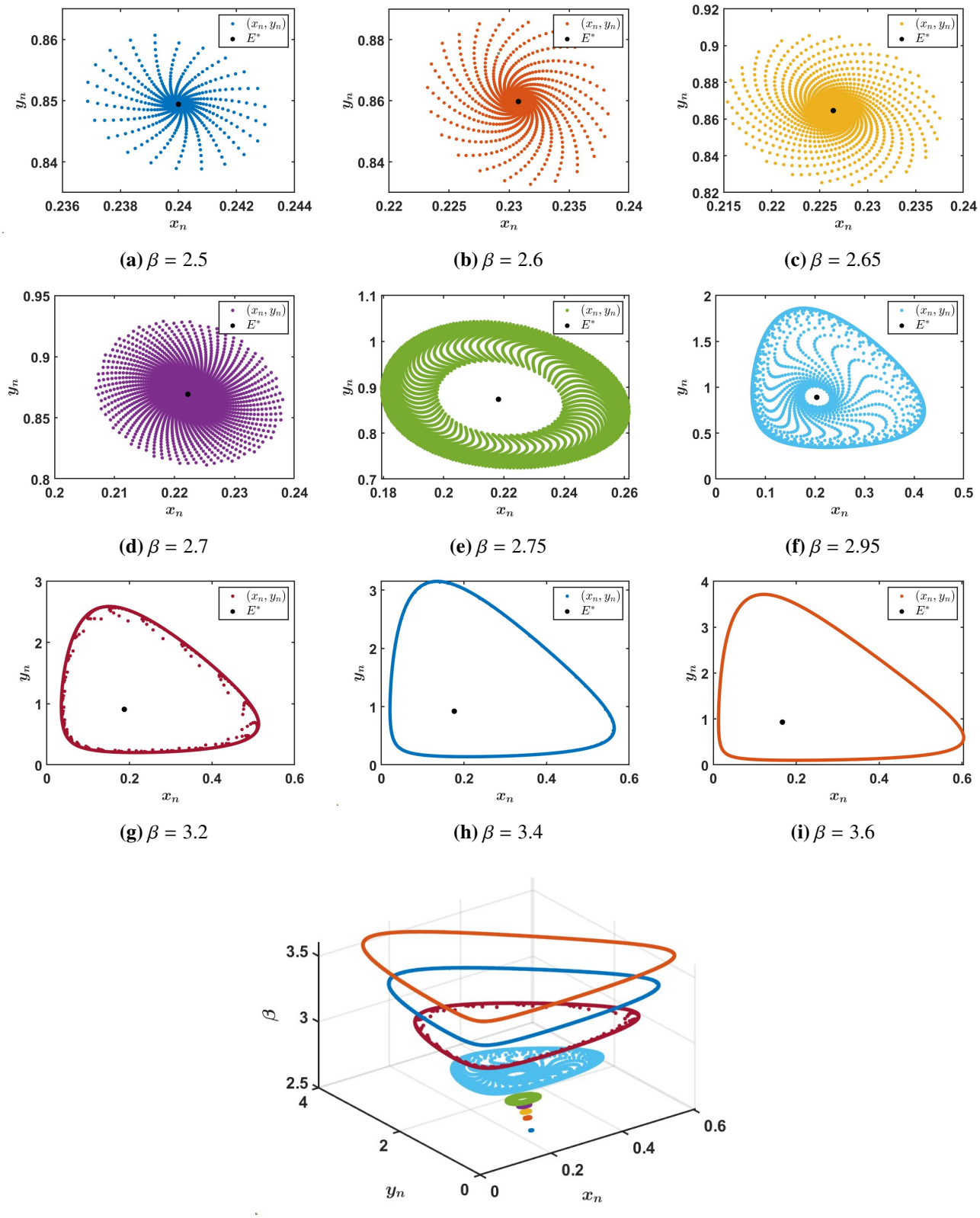

(a) $\beta = 2.5$ **(b)** $\beta = 2.6$ **(c)** $\beta = 2.65$

(d) $\beta = 2.7$ **(e)** $\beta = 2.75$ **(f)** $\beta = 2.95$

(g) $\beta = 3.2$ **(h)** $\beta = 3.4$ **(i)** $\beta = 3.6$

(j) 3D view of phase portraits

Figure 9. (a–i) Phase portraits of the system (1.3) are shown for different values of the parameter β with $\alpha = 0.95, \gamma = 0.85, \eta = 0.5, h = 0.10, \sigma = 0.65$, and initial conditions $x_0 = 0.2, y_0 = 0.9$ held fixed. (j) Three-dimensional representation of the phase portraits.

5.3. NS bifurcation analysis varying η, h and σ

Since the NS critical condition $\beta = 2(h + \eta) + \frac{1}{\sigma}$ only involves the parameters β, η, h, and σ, any of these parameters can be used to study the local stability of the coexistence equilibrium E^* and the oscillatory dynamics of system (1.3). In the context of the model, the parameters η and h jointly quantify the total per-capita loss rate of the predator population, where η and h account for natural and harvesting losses, respectively. Therefore, an increase in either of these parameters compromises the ability of the predator to persist and drives the system towards instability. Moreover, the parameter σ reflects the updating scale in the discrete formulation and may be viewed as an effective time-step or the seasonal interval separating successive population updates. Therefore, adjusting σ enables us to explore how the update frequency affects the initiation of oscillations in the predator-prey interaction.

5.3.1. Varying η

We set $\alpha = 0.95, \beta = 2.75, \gamma = 0.85, h = 0.10$, and $\sigma = 0.65$. For this choice of parameters, the critical value associated with the NS bifurcation is $\eta = 0.505769$. The associated interior equilibrium is $E^* = (0.22028, 0.871452)$. At this point, the Jacobian matrix admits a pair of complex conjugate eigenvalues $\xi_{1,2} = 0.957953 \pm 0.286926i$, whose modulus is equal to one. The bifurcation diagrams with respect to η over the interval $[0.01, 0.95]$ are displayed in Figure 10a and 10b, while corresponding MLE plot is shown in Figure 10c. Furthermore, Figure 11a–11i illustrate the phase portraits of system (1.3) for different values of η, and the corresponding three-dimensional representations are provided in Figure 11j.

The numerical results indicate that an increase in the predator mortality rate η can shift the system from oscillatory coexistence toward a stable equilibrium, while a decrease in η promotes the persistence of cycles following the destabilization of E^*. This demonstrates that changes in predator survival significantly influence whether the predator-prey system settles at a steady coexistence or exhibits sustained population oscillations.

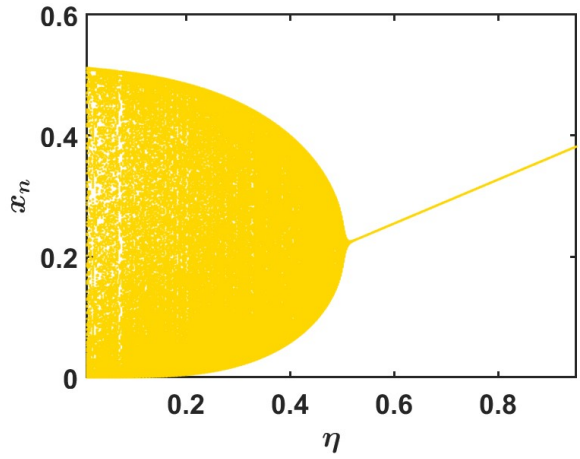

(a) Bifurcation diagram of x_n

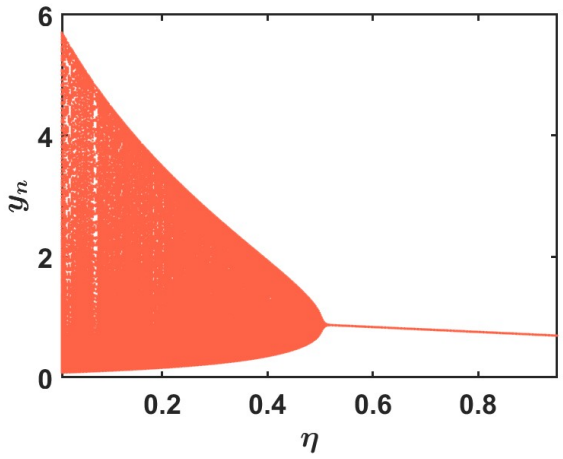

(b) Bifurcation diagram of y_n

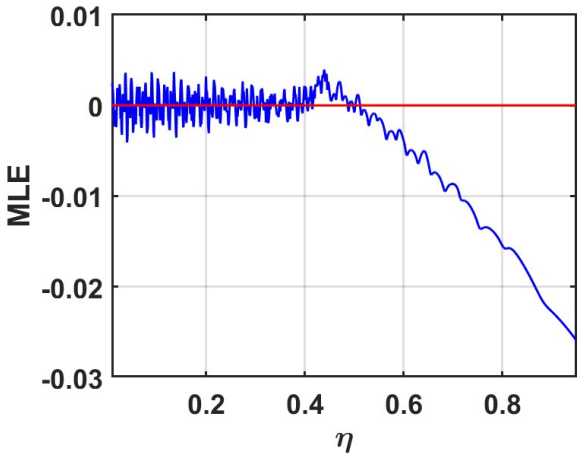

(c) MLE plot

Figure 10. Bifurcation diagrams together with the corresponding MLE plot of system (1.3) as the parameter η varies. The remaining parameters are fixed at $\alpha = 0.95, \beta = 2.75, \gamma = 0.85, h = 0.10$, and $\sigma = 0.65$, with initial conditions chosen as $x_0 = 0.2$, and $y_0 = 0.9$.

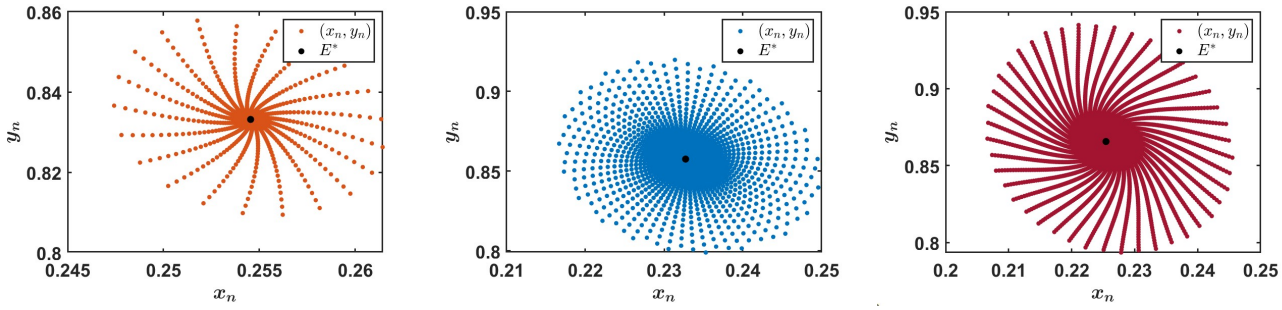

(a) $\eta = 0.60$

(b) $\eta = 0.54$

(c) $\eta = 0.52$

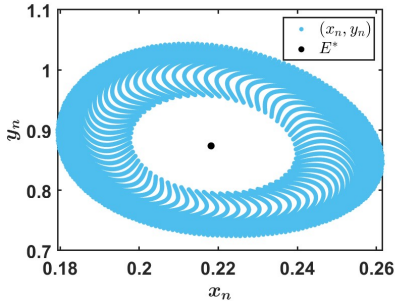

(d) $\eta = 0.50$

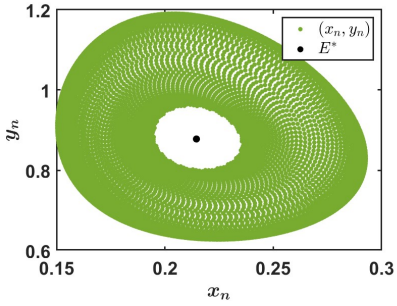

(e) $\eta = 0.49$

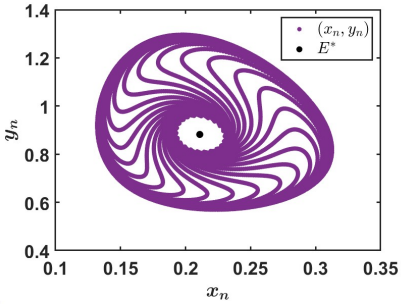

(f) $\eta = 0.48$

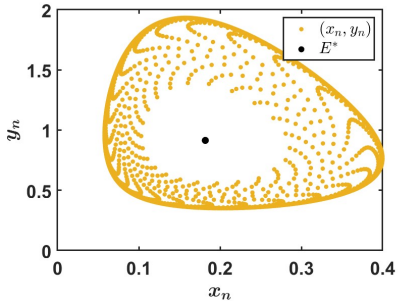

(g) $\eta = 0.40$

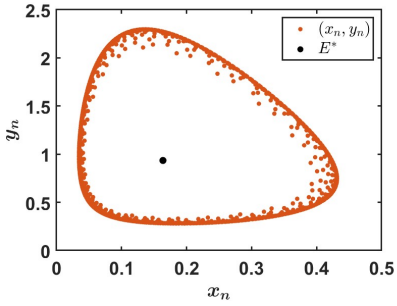

(h) $\eta = 0.35$

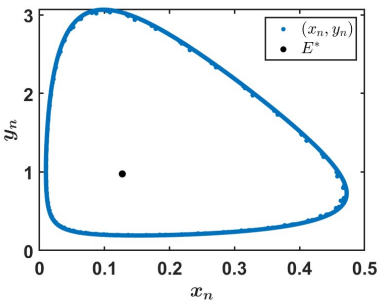

(i) $\eta = 0.25$

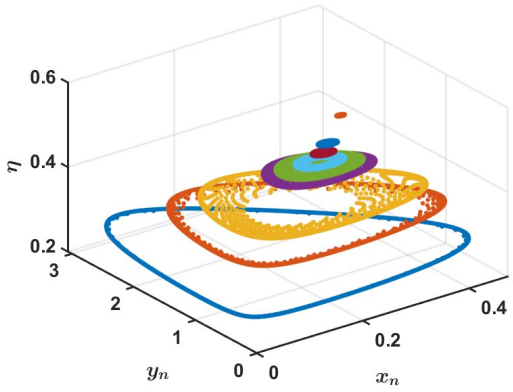

(j) 3D view of phase portraits

Figure 11. (a–i) Phase portraits of system (1.3) corresponding to various values of the parameter η with $\alpha = 0.95, \beta = 2.75, \gamma = 0.85, h = 0.10$, and $\sigma = 0.65$, and initial conditons $x_0 = 0.2, y_0 = 0.9$ held fixed. (j) Three-dimensional view of the associated phase portraits.

5.3.2. Varying h

We consider the parameter set $\alpha = 0.95, \beta = 2.75, \gamma = 0.85, \eta = 0.5$, and $\sigma = 0.65$. For this configuration, the critical value at which an NS bifurcation occurs is $h = 0.105769$. The associated coexistence equilibrium is $E^* = (0.22028, 0.871452)$. At this equilibrium, the Jacobian matrix possesses a pair of complex conjugate eigenvalues $\xi_{1,2} = 0.957953 \pm 0.286926i$, whose modulus is equal to one. Bifurcation diagrams corresponding to variations in h over the interval $[0.01, 0.35]$ are presented in Figure 12a and 12b, while the corresponding MLE plot is shown in Figure 12c. In addition, Figure 13a–13i display the phase portraits of system (1.3) for different values of h, and the corresponding three-dimensional visualization is provided in Figure 13j.

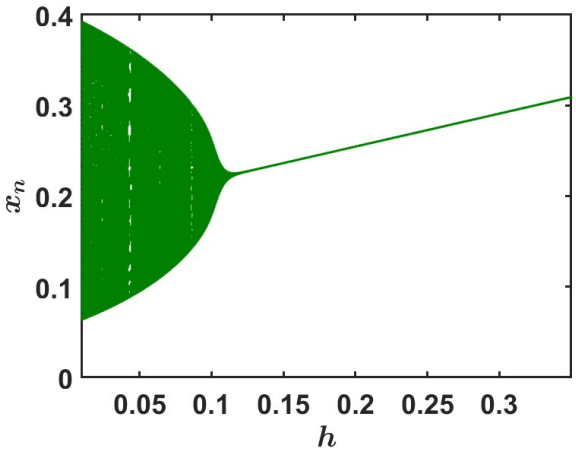

(a) Bifurcation diagram of x_n

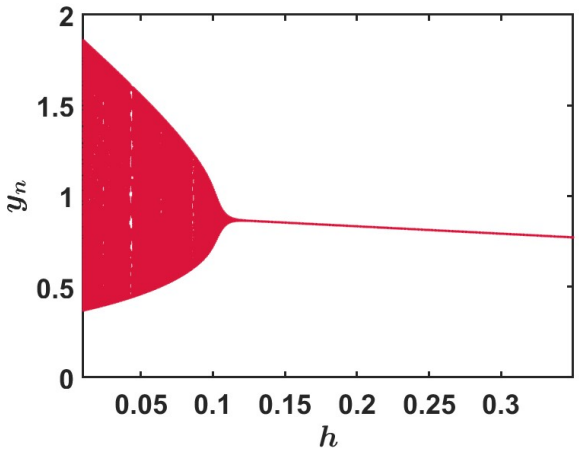

(b) Bifurcation diagram of y_n

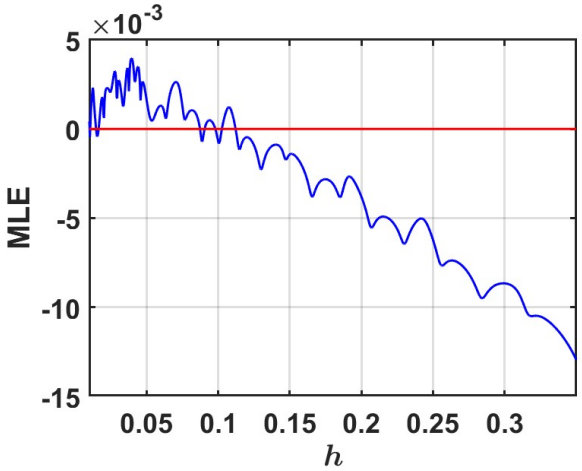

(c) MLE plot

Figure 12. Bifurcation diagrams and MLE plot of (1.3) varying h. Fixed parameter values are $\alpha = 0.95, \beta = 2.75, \gamma = 0.85, \eta = 0.5, \sigma = 0.65$, and initial conditions are $x_0 = 0.2, y_0 = 0.9$.

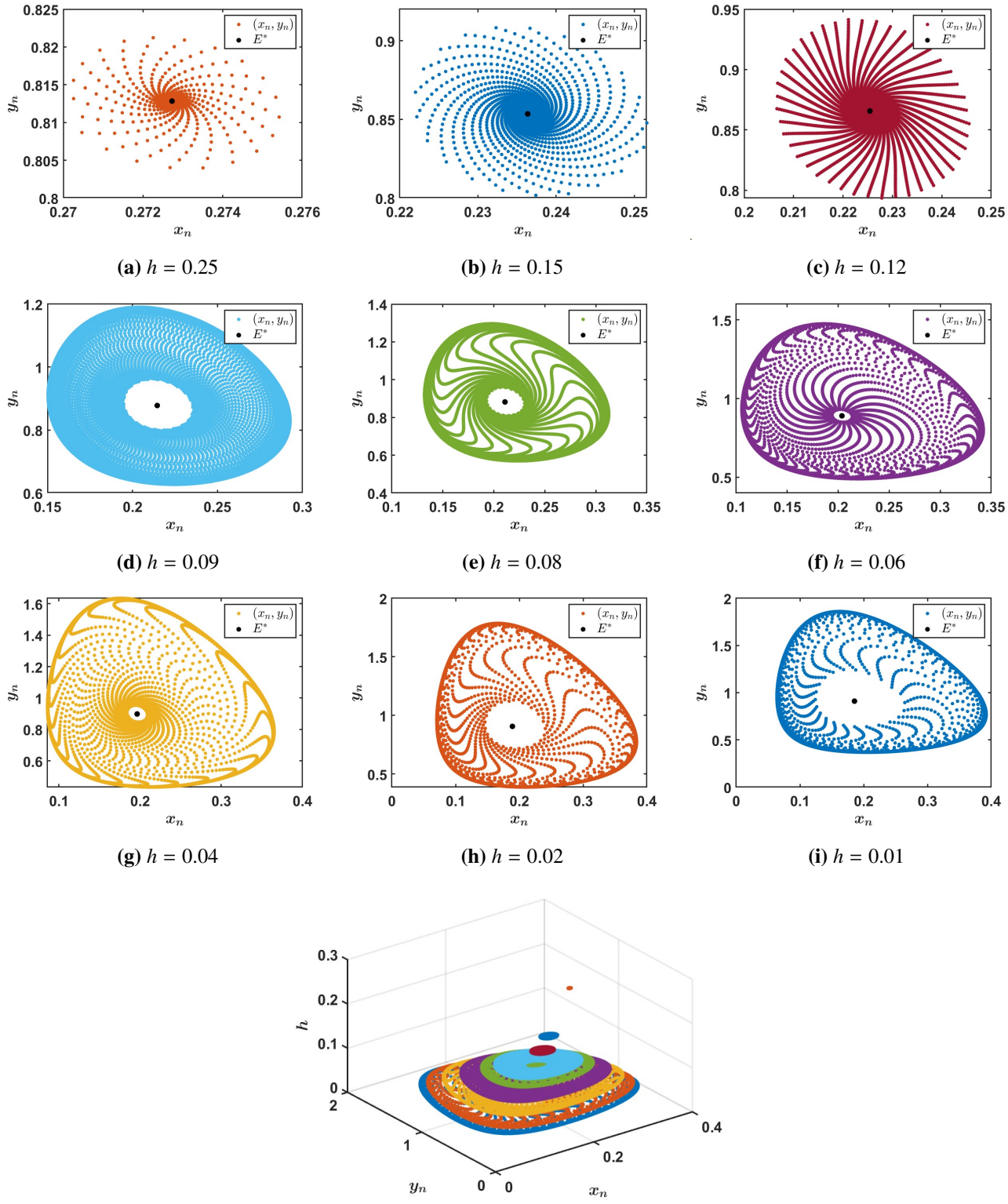

(a) $h = 0.25$ **(b)** $h = 0.15$ **(c)** $h = 0.12$

(d) $h = 0.09$ **(e)** $h = 0.08$ **(f)** $h = 0.06$

(g) $h = 0.04$ **(h)** $h = 0.02$ **(i)** $h = 0.01$

(j) 3D view of phase portraits

Figure 13. (a–i) Phase portraits of system (1.3) for various values of the parameter h with $\alpha = 0.95, \beta = 2.75, \gamma = 0.85, \eta = 0.5$, and $\sigma = 0.65$, and initial conditions $x_0 = 0.2, y_0 = 0.9$ kept fixed. (j) Three-dimensional representation of the corresponding phase portraits.

Ecologically, these outcomes indicate that predator harvesting can significantly modify the qualitative long-term behavior of the ecosystem. In particular, raising h generally weakens predator persistence and may promote equilibrium coexistence by attenuating oscillations. However, as the harvesting pressure gets closer to the NS threshold, there may be a transition from stable equilibrium coexistence to periodic oscillations. These periodic oscillations due to harvesting are particularly relevant in the context of wildlife and fish population management, as it has been observed that stable oscillations can increase the risk of extinction in the presence of environmental fluctuations.

5.3.3. Varying σ

We fix the parameters at $\alpha = 0.95, \beta = 2.75, \gamma = 0.85, \eta = 0.5$, and $h = 0.10$. Under these settings, the NS bifurcation occurs at the critical value $\sigma = 0.645161$. The associated interior equilibrium is $E^* = (0.218182, 0.873797)$. At this point, the Jacobean matrix admits a pair of complex conjugate eigenvalues $\xi_{1,2} = 0.958545 \pm 0.28494i$, whose modulus equals one. The bifurcation diagrams with respect to σ over the interval $[0.35, 1.35]$ are shown in Figure 14a, 14b, and the corresponding MLE plot is provided in Figure 14c. Furthermore, Figure 15a–15i illustrate the phase portraits of (1.3) for some values of σ, while the associated three-dimensional views are presented in Figure 15j.

From an ecological perspective, the importance of the σ parameter emphasizes the significance of the time scale in which population transitions occur in the asymptotic behavior of the system. In particular, after the NS bifurcation point, the value of σ indicates that the system could move from stable coexistence at equilibrium to periodic oscillations, implying that seasonal factors or delayed responses to demographic changes could cause periodic predator-prey interactions. This observation reinforces the idea that oscillatory coexistence may arise not only from the underlying ecological interactions, but also from the inherently discrete character of reproduction, recruitment, and population assessment in seasonal environments.

5.4. Codimension-two bifurcation analysis

In this section, we consider codimension-two bifurcations at positive fixed point E^* of system (1.3). For a detailed discussion of codimension-two bifurcations, readers are referred to [32–34]. We investigate 1:2, 1:3, and 1:4 resonances. The points of resonance are obtained by the following curves:

$$\begin{aligned} R_2 &: \alpha\sigma(-4\beta + \eta + h) = 4\beta, \\ R_3 &: \alpha\sigma(-3\beta + \eta + h) = 3\beta, \\ R_4 &: \alpha\sigma(-2\beta + \eta + h) = 2\beta, \\ NR &: \beta = 2(h + \eta) + \frac{1}{\sigma}. \end{aligned}$$

Intersections $R_2 \cap NR$, $R_3 \cap NR$, and $R_4 \cap NR$ identify parameter values at which 1:2, 1:3, and 1:4 resonances occur, respectively.

To determine whether strong resonance bifurcations can occur, we substitute the NS bifurcation condition

$$\beta = 2(h + \eta) + \frac{1}{\sigma}$$

into each resonance curve.

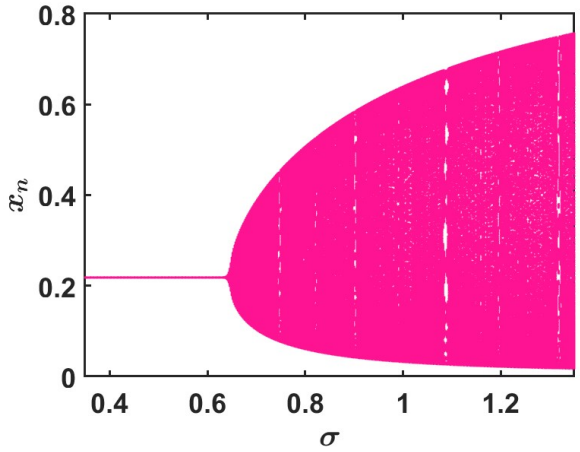

(a) Bifurcation diagram of x_n

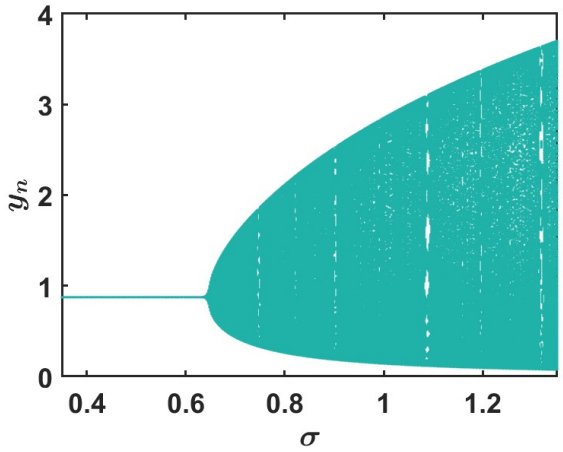

(b) Bifurcation diagram of y_n

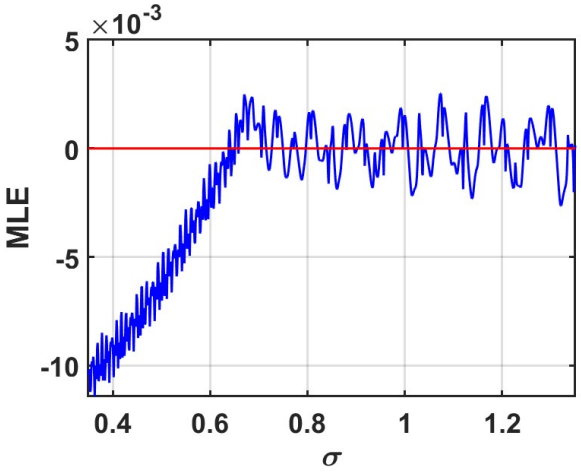

(c) MLE plot

Figure 14. Bifurcation diagrams together with the associated MLE plot of system (1.3) as the parameter σ varies. The remaining parameters are fixed at $\alpha = 0.95, \beta = 2.75, \gamma = 0.85, \eta = 0.5$, and $h = 0.10$, with initial conditions selected as $x_0 = 0.2$ and $y_0 = 0.9$.

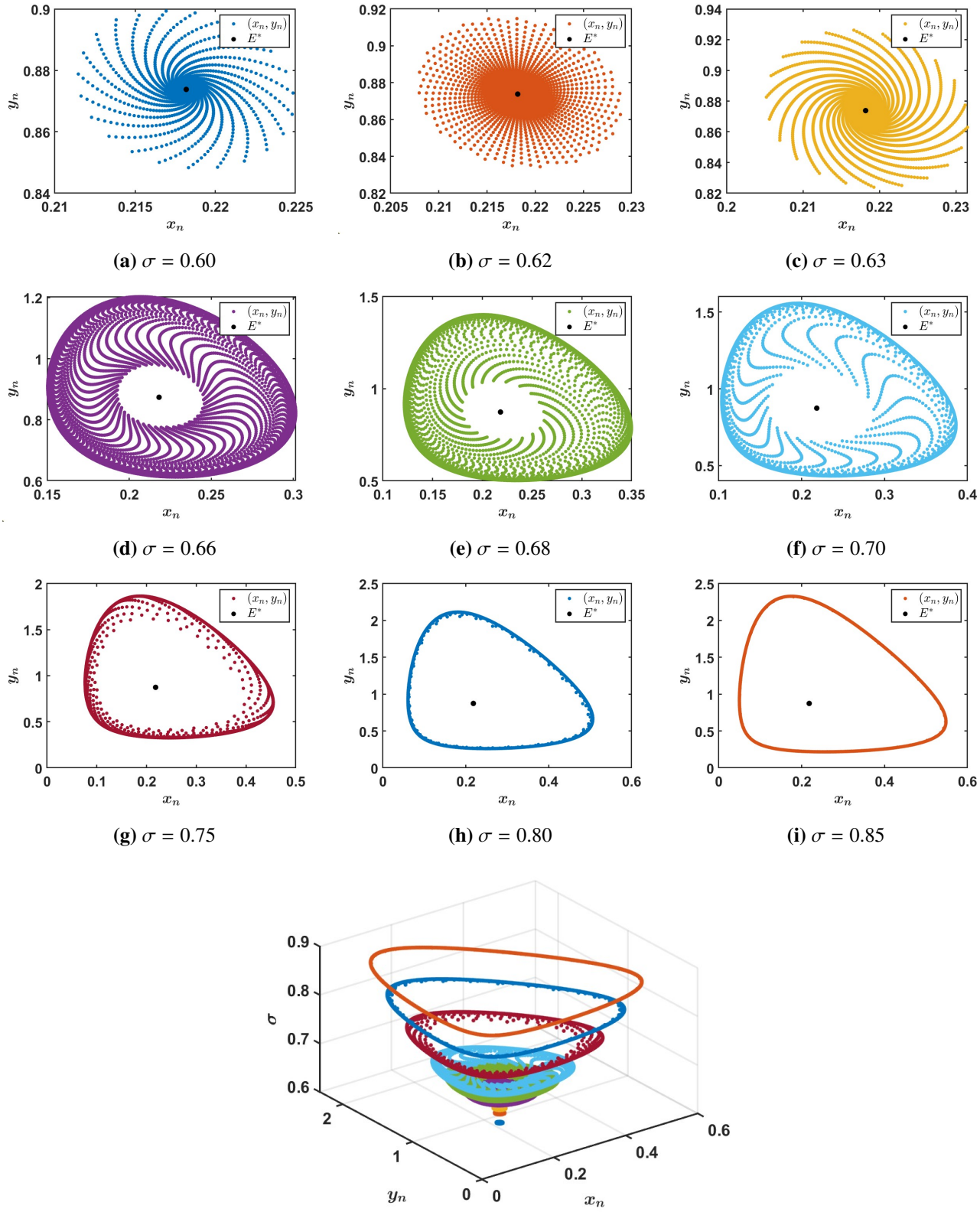

(a) $\sigma = 0.60$ **(b)** $\sigma = 0.62$ **(c)** $\sigma = 0.63$

(d) $\sigma = 0.66$ **(e)** $\sigma = 0.68$ **(f)** $\sigma = 0.70$

(g) $\sigma = 0.75$ **(h)** $\sigma = 0.80$ **(i)** $\sigma = 0.85$

(j) 3D view of phase portraits

Figure 15. (a–i) Phase portraits of (1.3) for different values of σ and fixing $\alpha = 0.95, \beta = 2.75, \gamma = 0.85, \eta = 0.5, h = 0.10, x_0 = 0.2$, and $y_0 = 0.9$. (j) 3D view of phase portraits.

For the 1:2 resonance curve R_2, this yields

$$\alpha\sigma\left[-7(h+\eta)-\frac{4}{\sigma}\right]=8(h+\eta)+\frac{4}{\sigma}.$$

The left-hand side is strictly negative, whereas the right-hand side is strictly positive for all admissible parameter values. Hence, no solution exists and $R_2 \cap NR = \emptyset$.

Similarly, substitution into R_3 gives

$$\alpha\sigma\left[-5(h+\eta)-\frac{3}{\sigma}\right]=6(h+\eta)+\frac{3}{\sigma},$$

whose left-hand side is negative and right-hand side positive. Therefore, $R_3 \cap NR = \emptyset$.

Finally, substitution into R_4 yields

$$\alpha\sigma\left[-3(h+\eta)-\frac{2}{\sigma}\right]=4(h+\eta)+\frac{2}{\sigma},$$

which again cannot be satisfied for positive parameters. Thus, $R_4 \cap NR = \emptyset$.

Therefore, codimension-two bifurcations do not occur at the positive fixed point E^* for the model (1.3). In contrast, the study in [22] analyzed the strong resonance bifurcations corresponding to the 1:2, 1:3, and 1:4 resonances.

6. Conclusions

In this paper, an NSFD discretization of a predator-prey model with predator harvesting is developed and analyzed. The proposed NSFD scheme preserves positivity of solutions and generates a discrete model that remains biologically meaningful for all admissible parameter values. The existence and local stability of all equilibrium points are established, and complete topological classifications of the fixed points are obtained through eigenvalue analysis. Furthermore, rigorous conditions for the occurrence of transcritical and NS bifurcations are derived, and the direction and stability of the bifurcating invariant curves are determined using normal form theory and the first Lyapunov coefficient.

The analysis demonstrates that the coexistence equilibrium can lose stability through an NS bifurcation, leading to sustained oscillatory behavior represented by invariant closed curves. In contrast to [22], PD and strong resonance bifurcations are excluded at the coexistence equilibrium, indicating that the proposed discretization avoids some common routes to discretization-induced complex dynamics. Numerical investigations support theoretical results and provided additional insight into the long-term behavior of the system.

A further contribution of this work is the incorporation of machine learning techniques into the study of discrete ecological dynamics. Decision tree, random forest, and SVM classifiers are successfully employed to predict both the topological nature of the positive equilibrium and the long-term dynamical behavior of the system over large parameter domains. The high classification accuracies obtained by these methods demonstrate that machine learning can serve as an effective computational tool for exploring complex dynamical systems and can complement traditional analytical approaches. These findings are consistent with recent machine learning-based studies of discrete ecological systems [20, 21]. Similar to the results reported in [20], random forest provides the best classification

performance in the present study, while our analysis further considers the classification of long-term periodic, quasiperiodic, and chaotic dynamics.

These results highlight the effectiveness of the NSFD methodology in constructing dynamically consistent discrete ecological models while illustrating the potential of machine learning as a supplementary framework for dynamical classification and prediction.

Author contributions

Asifa Tassaddiq: Investigation, Methodology, Software, Writing–original draft. Rizwan Ahmed: Conceptualization, Investigation, Methodology, Supervision, Writing–original draft. Rabab Alharbi: Formal analysis, Software, Validation, Writing–review and editing. Dalal Khalid Almutairi: Investigation, Software, Writing–review and editing. Ruhaila Md Kasmani: Formal analysis, Validation, Writing–review and editing. Youngmoon Lee: Conceptualization, Methodology, Supervision, Data Curation. Jawad Khan: Formal analysis, Validation, Data Curation.

Acknowledgments

The authors extend their appreciation to the Deanship of Postgraduate Studies and Scientific Research at Majmaah University for funding this research work through the project number (ICR-2026-368). This work was supported in part by the National Research Foundation of Korea (NRF) grant RS-2026-25468407 and Institute of Information and Communications Technology Planning and Evaluation (IITP) grant RS-2026-25616659, RS-2026-25547714 all funded by Ministry of Science and Information and Communications Technology, Korea.

Conflict of interest

The authors have no conflicts of interest to disclose.

Use of Generative-AI tools declaration

The authors declare they have not used Artificial Intelligence (AI) tools in the creation of this article.

References

1. A. J. Lotka, Elements of physical biology, *Nature*, **116** (1925), 461. https://doi.org/10.1038/116461b0
2. V. Volterra, Fluctuations in the abundance of a species considered mathematically, *Nature*, **118** (1926), 558–560. https://doi.org/10.1038/119012b0
3. S. M. S. Rana, Bifurcation and complex dynamics of a discrete-time predator-prey system with simplified Monod-Haldane functional response, *Adv. Differ. Equ-NY.*, **2015** (2015), 345. https://doi.org/10.1186/s13662-015-0680-7

4. M. B. Almatrafi, M. Berkal, R. Ahmed, Dynamical transitions and chaos control in a discrete predator-prey model with Gompertz growth and Holling type III response, *Chaos, Soliton. Fract.*, **200** (2025), 117071. https://doi.org/10.1016/j.chaos.2025.117071
5. Z. Ma, W. Li, Y. Zhao, W. Wang, H. Zhang, Z. Li, Effects of prey refuges on a predator-prey model with a class of functional responses: The role of refuges, *Math. Biosci.*, **218** (2009), 73–79. https://doi.org/10.1016/j.mbs.2008.12.008
6. S. Khajanchi, S. Banerjee, Role of constant prey refuge on stage structure predator-prey model with ratio dependent functional response, *Appl. Math. Comput.*, **314** (2017), 193–198. https://doi.org/10.1016/j.amc.2017.07.017
7. R. Ahmed, M. S. Yazdani, S. Saher, Complex dynamics of a predator-prey model with harvesting effects on both predator and prey, *Int. J. Nonlinear Anal.*, **14** (2023), 95–106. https://doi.org/10.5890/jand.2023.09.004
8. D. Sen, S. Ghorai, M. Banerjee, A. Morozov, Bifurcation analysis of the predator-prey model with the Allee effect in the predator, *J. Math. Biol.*, **84** (2022), 7. https://doi.org/10.1007/s00285-021-01707-x
9. H. Deng, F. Chen, Z. Zhu, Z. Li, Dynamic behaviors of Lotka-Volterra predator-prey model incorporating predator cannibalism, *Adv. Differ. Equ-NY.*, **2019** (2019) 359. https://doi.org/10.1186/s13662-019-2289-8
10. Q. Din, K. Jameel, M. S. Shabbir, Discrete-time predator-prey system incorporating fear effect: Stability, bifurcation, and chaos control, *Qual. Theor. Dyn. Syst.*, **23** (2024), 285. https://doi.org/10.1007/s12346-024-01145-2
11. A. Tassaddiq, R. Ahmed, A. Ditta, Exploring stability and bifurcation in a discretized commensalism model, *Nonlinear Dynam.*, **113** (2025), 28463–28475. https://doi.org/10.1007/s11071-025-11530-4
12. R. E. Mickens, *Nonstandard Finite Difference Models of Differential Equations*, World Scientific, 1993. https://doi.org/10.1142/2081
13. R. E. Mickens, A nonstandard finite-difference scheme for the Lotka-Volterra system, *Appl. Numer. Math.*, **45** (2003), 309–314. https://doi.org/10.1016/s0168-9274(02)00223-4
14. S. Moghadas, M. Alexander, B. Corbett, A non-standard numerical scheme for a generalized Gause-type predator-prey model, *Physica D*, **188** (2004), 134–151. https://doi.org/10.1016/S0167-2789(03)00285-9
15. N. Bairagi, M. Biswas, A predator-prey model with Beddington-DeAngelis functional response: A non-standard finite-difference method, *J. Differ. Equ. Appl.*, **22** (2015), 581–593. https://doi.org/10.1080/10236198.2015.1111345
16. M. S. Shabbir, Q. Din, M. Safeer, M. A. Khan, K. Ahmad, A dynamically consistent nonstandard finite difference scheme for a predator-prey model, *Adv. Differ. Equ-NY.*, **2019** (2019), 381. https://doi.org/10.1186/s13662-019-2319-6
17. Q. A. Dang, M. T. Hoang, Nonstandard finite difference schemes for a general predator-prey system, *J. Comput. Sci.*, **36** (2019), 101015. https://doi.org/10.1016/j.jocs.2019.07.002

18. R. Ahmed, A. Ahmad, N. Ali, Stability analysis and Neimark-Sacker bifurcation of a nonstandard finite difference scheme for Lotka-Volterra prey-predator model, *Commun. Math. Biol. Neu.*, **2022** (2022), 61. https://doi.org/10.28919/cmbn/7534

19. C. Kome, Y. Yazlik, Stability, bifurcation analysis and chaos control in a discrete predator-prey system incorporating prey immigration, *J. Appl. Math. Comput.*, **70** (2024), 5213–5247. https://doi.org/10.1007/s12190-024-02230-0

20. T. Mehmood, M. Rafaqat, S. Saleem, F. E. Merga, Machine learning and bifurcation analysis in a discrete predator-prey model with neem-induced mortality, *Sci. Rep.*, **15** (2025), 40792. https://doi.org/10.1038/s41598-025-24544-0

21. A. K. Sethy, J. Datta, R. K. Upadhyay, Exploring the complex and nonlinear dynamics in discrete ecological systems: A machine learning approach, *Chaos, Soliton. Fract.*, **211** (2026), 118865. https://doi.org/10.1016/j.chaos.2026.118865

22. V. S. Sharma , A. Singh, Strong resonance bifurcations and state feedback control in a discrete prey-predator model with harvesting effect, *Qual. Theor. Dyn. Syst.*, **22** (2023), 109. https://doi.org/10.1007/s12346-023-00805-z

23. V. S. Sharma, A. Singh, A. Elsonbaty, A. A. Elsadany, Codimension-one and -two bifurcation analysis of a discrete-time prey-predator model, *Int. J. Dynam. Control*, **11** (2023), 2691–2705. https://doi.org/10.1007/s40435-023-01177-7

24. S. F. Aldosary, R. Ahmed, Stability and bifurcation analysis of a discrete Leslie predator-prey system via piecewise constant argument method, *AIMS Math.*, **9** (2024), 4684–4706. https://doi.org/10.3934/math.2024226

25. W. Ishaque, Q. Din, K. A. Khan, R. M. Mabela, Dynamics of predator-prey model based on fear effect with bifurcation analysis and chaos control, *Qual. Theor. Dyn. Syst.*, **23** (2023), 26. https://doi.org/10.1007/s12346-023-00878-w

26. Y. Liu, L. Guo, X. Liu, Multiple bifurcation analysis in a discrete-time predator-prey model with holling IV response function, *Symmetry*, **17** (2025), 1459. https://doi.org/10.3390/sym17091459

27. W. Ishaque, Q. Din, Refuge-mediated stability and codimension-two bifurcation in a discrete Leslie-Gower predator-prey system, *Int. J. Dyn. Control*, **13** (2025), 419. https://doi.org/10.1007/s40435-025-01933-x

28. A. Tassaddiq, A. Mehmood, R. Ahmed, Impact of carrying capacity on the dynamics of a discrete-time plant-herbivore system, *Chaos, Soliton. Fract.*, **201** (2025), 117284. https://doi.org/10.1016/j.chaos.2025.117284

29. J. Guckenheimer, P. Holmes, *Nonlinear Oscillations, Dynamical Systems, and Bifurcations of Vector Fields*, 42. Springer New York, 1983. https://doi.org/10.1007/978-1-4612-1140-2

30. S. Wiggins, M. Golubitsky, *Introduction to Applied Nonlinear Dynamical Systems and Chaos*, 2. Springer-Verlag, 2003. https://doi.org/10.1007/b97481

31. Y. A. Kuznetsov, *Elements of Applied Bifurcation Theory*, 112. Springer New York, 2004. https://doi.org/10.1007/978-1-4757-3978-7

32. B. Li, Z. Eskandari, Z. Avazzadeh, Strong resonance bifurcations for a discrete-time prey-predator model, *J. Appl. Math. Comput.*, **69** (2023), 2421–2438. https://doi.org/10.1007/s12190-023-01842-2

33. R. K. Ghaziani, W. Govaerts, C. Sonck, Resonance and bifurcation in a discrete-time predator-prey system with Holling functional response, *Nonlinear Anal-Real*, **13** (2012), 1451–1465. https://doi.org/10.1016/j.nonrwa.2011.11.009

34. J. G. Wang, X. Y. Meng, L. Lv, J. Li, Stability and bifurcation analysis of a Beddington-DeAngelis prey-predator model with fear effect, prey refuge and harvesting, *Int. J. Bifurcat. Chaos*, **33** (2023), 2350013. https://doi.org/10.1142/S021812742350013X

Appendix

A. Nonlinear term coefficients in the system (3.7)

$$a_1 = \frac{\alpha\sigma(-1-\sigma(2h+\alpha+\delta+2\eta+\alpha(h+\delta+\eta)\sigma))}{(1+\alpha\sigma)^2(1+(2h+\delta+2\eta)\sigma)},\ a_2 = \frac{\gamma^2(h+\eta)\sigma^3}{(1+\alpha\sigma)^2(1+(2h+\delta+2\eta)\sigma)},$$

$$a_3 = -\frac{\gamma\sigma(1+\sigma(2h+\alpha+\delta+2\eta+\alpha\delta\sigma))}{(1+\alpha\sigma)^2(1+(2h+\delta+2\eta)\sigma)},\ a_4 = \frac{\alpha^2\sigma^2(1+\sigma(2h+\alpha+\delta+2\eta+\alpha(h+\delta+\eta)\sigma))}{(1+\alpha\sigma)^3(1+(2h+\delta+2\eta)\sigma)},$$

$$a_5 = -\frac{\gamma^3(h+\eta)\sigma^4}{(1+\alpha\sigma)^3(1+(2h+\delta+2\eta)\sigma)},\ a_6 = \frac{\alpha\gamma\sigma^2(2+2(2h+\alpha+\delta+2\eta)\sigma+\alpha(h+2\delta+\eta)\sigma^2)}{(1+\alpha\sigma)^3(1+(2h+\delta+2\eta)\sigma)},$$

$$a_7 = \frac{\gamma^2\sigma^2(1+\sigma(2h+\alpha+\delta+2\eta-\alpha(h-\delta+\eta)\sigma))}{(1+\alpha\sigma)^3(1+(2h+\delta+2\eta)\sigma)}.$$

B. Coefficients associated with the nonlinear terms of the system (3.11)

$$c_1 = \frac{\alpha\gamma(h+\eta)\sigma^3(2+4\eta\sigma+h\sigma(4+3\alpha\sigma)+\alpha\sigma(2+3\eta\sigma))}{4(1+\alpha\sigma)^3(1+2h\sigma+2\eta\sigma)^2},$$

$$c_2 = -\frac{\alpha\gamma(h+\eta)\sigma^3(4+4(2h+\alpha+2\eta)\sigma+7\alpha(h+\eta)\sigma^2)}{4(1+\alpha\sigma)^3(1+2(h+\eta)\sigma)^2},$$

$$c_3 = \frac{\gamma\sigma^2(1+2\eta\sigma+h\sigma(2+\alpha\sigma)+\alpha\sigma(1+\eta\sigma))\sqrt{\alpha(h+\eta)(4+8\eta\sigma+h\sigma(8+7\alpha\sigma)+\alpha\sigma(4+7\eta\sigma))}}{2(1+\alpha\sigma)^3(1+2h\sigma+2\eta\sigma)^2},$$

$$c_4 = \frac{\alpha^2\gamma^2(h+\eta)^2\sigma^6(2+4\eta\sigma+h\sigma(4+3\alpha\sigma)+\alpha\sigma(2+3\eta\sigma))}{8(1+\alpha\sigma)^5(1+2h\sigma+2\eta\sigma)^3},$$

$$c_5 = -\frac{\gamma^2\sigma^5(\alpha(h+\eta)(4+8\eta\sigma+h\sigma(8+7\alpha\sigma)+\alpha\sigma(4+7\eta\sigma)))^{3/2}}{8(1+\alpha\sigma)^5(1+2h\sigma+2\eta\sigma)^3},$$

$$c_6 = \frac{\alpha\gamma^2(h+\eta)\sigma^5(4+8\eta\sigma+h\sigma(8+5\alpha\sigma)+\alpha\sigma(4+5\eta\sigma))\sqrt{\alpha(h+\eta)(4+8\eta\sigma+h\sigma(8+7\alpha\sigma)+\alpha\sigma(4+7\eta\sigma))}}{8(1+\alpha\sigma)^5(1+2h\sigma+2\eta\sigma)^3},$$

$$c_7 = \frac{\alpha\gamma^2(h+\eta)\sigma^4(2+4\eta\sigma+h\sigma(4+\alpha\sigma)+\alpha\sigma(2+\eta\sigma))(4+8\eta\sigma+h\sigma(8+7\alpha\sigma)+\alpha\sigma(4+7\eta\sigma))}{8(1+\alpha\sigma)^5(1+2h\sigma+2\eta\sigma)^3},$$

$$d_1 = \frac{\left\{\begin{array}{l}(\alpha\gamma(h+\eta)^2\sigma^3(4(1+2\eta\sigma)^2+h^2\sigma^2(16+36\alpha\sigma+19\alpha^2\sigma^2)+2\alpha\sigma(5+19\eta\sigma+18\eta^2\sigma^2)\\+\alpha^2\sigma^2(6+21\eta\sigma+19\eta^2\sigma^2)+h\sigma(16+32\eta\sigma+2\alpha\sigma(19+36\eta\sigma)+\alpha^2\sigma^2(21+38\eta\sigma))))\end{array}\right\}}{(4(1+\alpha\sigma)^3(1+h\sigma+\eta\sigma)(1+2h\sigma+2\eta\sigma)^2\sqrt{\alpha(h+\eta)(4+8\eta\sigma+h\sigma(8+7\alpha\sigma)+\alpha\sigma(4+7\eta\sigma))})},$$

$$d_2 = -\frac{\alpha\gamma(h+\eta)\sigma^4\sqrt{\alpha(h+\eta)(4+8\eta\sigma+h\sigma(8+7\alpha\sigma)+\alpha\sigma(4+7\eta\sigma))}}{4(1+\alpha\sigma)^3(1+2h\sigma+2\eta\sigma)^2},$$

$$d_3 = \frac{\left\{\begin{array}{l}-(\gamma(h+\eta)\sigma^2(2(1+2\eta\sigma)^2+h^2\sigma^2(8+14\alpha\sigma+7\alpha^2\sigma^2)+\alpha^2\sigma^2(1+6\eta\sigma+7\eta^2\sigma^2)+\alpha\sigma(3+13\eta\sigma\\+14\eta^2\sigma^2)+h\sigma(8+16\eta\sigma+2\alpha^2\sigma^2(3+7\eta\sigma)+\alpha\sigma(13+28\eta\sigma))))\end{array}\right\}}{(2(1+\alpha\sigma)^3(1+h\sigma+\eta\sigma)(1+2h\sigma+2\eta\sigma)^2)},$$

$$d_4 = \frac{\alpha^3\gamma^2(h+\eta)^3\sigma^7(2+4\eta\sigma+h\sigma(4+3\alpha\sigma)+\alpha\sigma(2+3\eta\sigma))}{8(1+\alpha\sigma)^5(1+2h\sigma+2\eta\sigma)^3\sqrt{\alpha(h+\eta)(4+8\eta\sigma+h\sigma(8+7\alpha\sigma)+\alpha\sigma(4+7\eta\sigma))}},$$

$$d_5 = -\frac{\alpha^2\gamma^2(h+\eta)^2\sigma^6(4+8\eta\sigma+h\sigma(8+7\alpha\sigma)+\alpha\sigma(4+7\eta\sigma))}{8(1+\alpha\sigma)^5(1+2h\sigma+2\eta\sigma)^3},$$

$$d_6 = \frac{\alpha^2\gamma^2(h+\eta)^2\sigma^6(4+8\eta\sigma+h\sigma(8+5\alpha\sigma)+\alpha\sigma(4+5\eta\sigma))}{8(1+\alpha\sigma)^5(1+2h\sigma+2\eta\sigma)^3},$$

$$d_7 = \frac{\alpha\gamma^2(h+\eta)\sigma^5(2+4\eta\sigma+h\sigma(4+\alpha\sigma)+\alpha\sigma(2+\eta\sigma))\sqrt{\alpha(h+\eta)(4+8\eta\sigma+h\sigma(8+7\alpha\sigma)+\alpha\sigma(4+7\eta\sigma))}}{8(1+\alpha\sigma)^5(1+2h\sigma+2\eta\sigma)^3}.$$